A review of nonlinear fluid models for ion-and electron-acoustic solitons and double layers: Application to weak double layers and electrostatic solitary waves in the solar wind and the lunar wake

G. S. Lakhina, S. V. Singh, R. Rubia, and T. Sreeraj

Citation: Physics of Plasmas **25**, 080501 (2018); doi: 10.1063/1.5033498
View online: https://doi.org/10.1063/1.5033498
View Table of Contents: http://aip.scitation.org/toc/php/25/8
Published by the American Institute of Physics

A review of nonlinear fluid models for ion-and electron-acoustic solitons and double layers: Application to weak double layers and electrostatic solitary waves in the solar wind and the lunar wake

G. S. Lakhina,[a] S. V. Singh,[b] R. Rubia,[c] and T. Sreeraj[d]
Indian Institute of Geomagnetism, Plot No. 5, Sector-18, New Panvel (W), Navi Mumbai 410218, India

(Received 6 April 2018; accepted 5 July 2018; published online 1 August 2018)

Electrostatic solitary waves (ESWs) have been observed in the Earth's magnetosphere, solar wind, lunar wake, and also in other planetary magnetospheres. The observed characteristics of the ESWs have been interpreted in terms of models based either on Bernstein-Green-Kruskal (BGK) modes/phase space holes or ion- and electron-acoustic solitons. However, the space community has favored the models based on BGK modes/phase space holes. In this review, current understanding of the fluid models for ion-and electron-acoustic solitons and double layers in multi-component plasmas is presented. The relationship between the theoretical models and space observations of ESWs is emphasized. Two specific applications of ion- and electron-acoustic solitons to the occurrence of weak double layers and coherent electrostatic waves in the solar wind and the lunar wake are discussed by comparing the observations and theoretical predictions. It is concluded that models based on ion- and electron-acoustic solitons/double layers provide a plausible interpretation for the ESWs observed in space plasmas. *Published by AIP Publishing.*
https://doi.org/10.1063/1.5033498

I. INTRODUCTION

Broadband electrostatic noise (BEN), having frequencies in the range of ion cyclotron frequency and local electron plasma frequency (or even above), has been generally recorded in every magnetosphere flow boundary where spacecraft wave measurements have been made to date. For example, BEN has been observed at the magnetopause,[1] in the neutral sheet,[2] plasma sheet boundary layer (PSBL),[3] magnetotail,[4,5] polar cap boundary layer (PCBL),[6] bow-shock,[7,8] magnetosheath,[9,10] and on cusp and auroral zone field lines at various altitudes.[4,11–16] BEN is usually associated with ion and/or electron beams, and its spectrum follows a power law. Eastman *et al.*[17] have suggested that BEN could be the source of hot ions in the central plasma sheet (CPS).

Figure 1 shows plasma wave electric and magnetic field data at the magnetopause from the International Sun-Earth Explorer 1 (ISEE-1) on November 10, 1977, as reported for the first time by Gurnett *et al.*[1] The electric field sensors covered the frequency range from 5.6 Hz to 311 kHz, and the magnetic field sensors covered the frequency range from 5.6 Hz to 3.11 kHz. The locations of the bow shock and the magnetopause (both inbound and outbound) are marked by the vertical dashed lines in the figure. It is seen from Fig. 1 that maximum intensities of the plasma waves usually occur at the magnetopause. Gurnett *et al.*[1] observed that electric (E) waves extend over a wide range from 5.6 Hz to 100 kHz and their spectra follow a $f^{-2.2}$ power law. The magnetic (B) waves, however, extend from 5.6 Hz to 1 kHz, and they had a $f^{-3.3}$ power law spectrum. The frequency dependence and the amplitude ratio of wave magnetic to electric field, i.e., B/E ratio, suggest that the waves are most likely a mixture of electrostatic and electromagnetic (whistler) modes.[1,18]

Figure 2 shows a frequency-time color spectrogram of the polar cap boundary layer (PCBL) wave from the polar plasma wave multichannel analyzer data obtained on April 7, 1996. The Polar spacecraft orbit has an inclination of 86° with an apogee of ~9 R_E and a perigee of ~1.8 R_E and covers the noon-midnight sector.[6] Here, R_E stands for the Earth's radius. The plot shown in Fig. 2 covers 24 h (horizontal axis) and a frequency range of 5 Hz to 311 kHz (vertical axis). The electric field (E) power spectral density is plotted according to the color bar to the right of the spectrogram. The universal time (UT), radial distance from the center of the earth (R_E), magnetic latitude (M), magnetic local time (MLT), and approximate L shell value are shown at the bottom of the plot. In Fig. 2, the wave intervals of interest are indicated by two sets of arrows along the time axis and are labeled as "Dayside PCBL" and "Nightside PCBL." Since the intervals of intense broadband plasma waves are found to bind magnetic fields that map into the polar cap region, hence the name PCBL waves. The PCBL waves are characterized by bursts of "turbulence" covering a broad frequency range extending from $f < 10^1$ to 2×10^4 Hz as seen from Fig. 2. The magnetic field spectrum for these waves shows similar bursts (see Ref. 6). The region of intense PCBL waves maps to the low latitude boundary layer. Further, the PCBL waves are spiky and their frequency dependence and intensities are quite similar to those detected at or near the magnetopause.[1,19]

Figure 3 shows the first observation of double layers (DL) and solitary waves (SW) having electric field component parallel to the magnetic field, occurring in the auroral acceleration region between 6000 and 8000 km altitude, reported by Temerin *et al.*[20] from the S3-3 spacecraft. Three components of the electric field in the magnetic field-aligned

[a]Electronic mail: gslakhina@gmail.com
[b]Electronic mail: satyavir@iigs.iigm.res.in
[c]Electronic mail: rubi.r92@gmail.com
[d]Electronic mail: sreerajt90@gmail.com

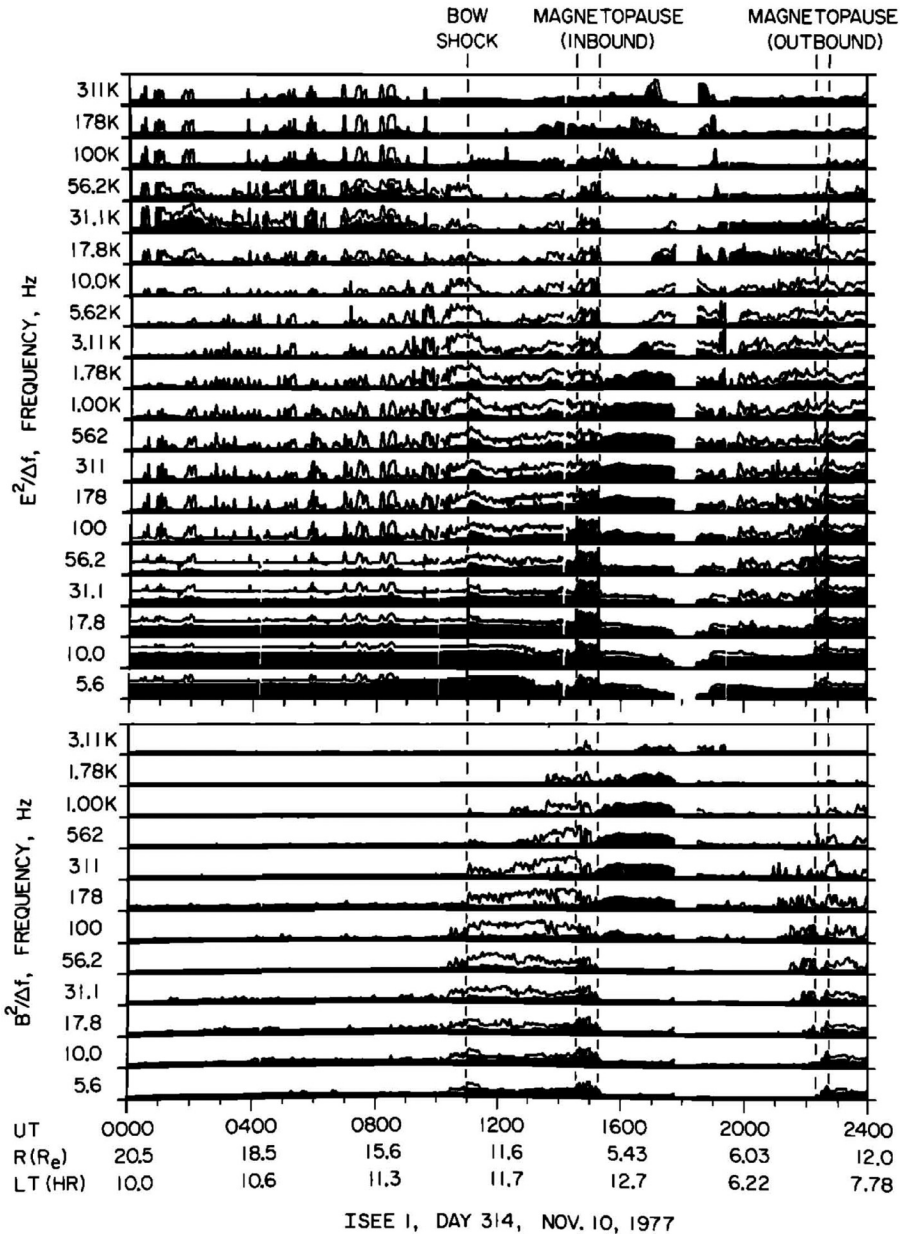

FIG. 1. The plasma wave electric and magnetic field data from ISEE 1 for a representative pass through the magnetosphere. The enhanced electric and magnetic field intensities at the inbound and outbound magnetopause crossing are clearly evident. Reprinted with permission from Gurnett *et al.*, J. Geophys. Res. **84**(A12), 7043–7058 (1979). Copyright John Wiley and Sons.[1]

coordinates for two events 2 s apart are shown in this figure. The examples of DL and SW in the parallel electric field component are marked with negative electric field pointing out of the ionosphere in both the panels. The parallel electric fields are typically $\sim$10 mV m^{-1} with durations of a few ms. The perpendicular electric field components show the presence of electrostatic ion-cyclotron (EIC) waves at a frequency of $\sim$140 Hz. The two examples shown in Fig. 3 form a small portion of $\sim$400 double layers and solitary waves observed in the 45 s interval that coincided with a region of

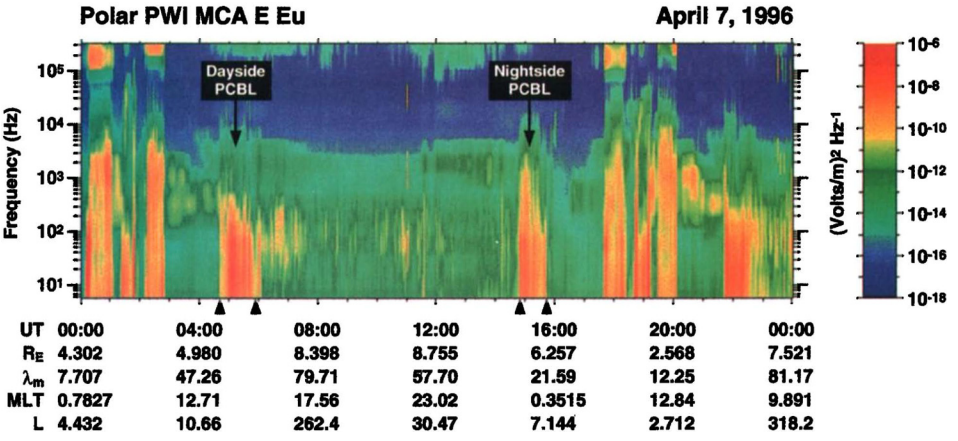

FIG. 2. Color spectrogram of wave electric field from $\sim 10^1$ to 10^5 Hz and above. The boundary layer waves are indicated by arrows. In between the two boundary layers (dayside and nightside) crossings is the polar cap (quiet wave region). Reprinted with permission from Tsurutani *et al.*, J. Geophys. Res. **103**(A8), 17351–17366 (1988). Copyright 1988 John Wiley and Sons.[6]

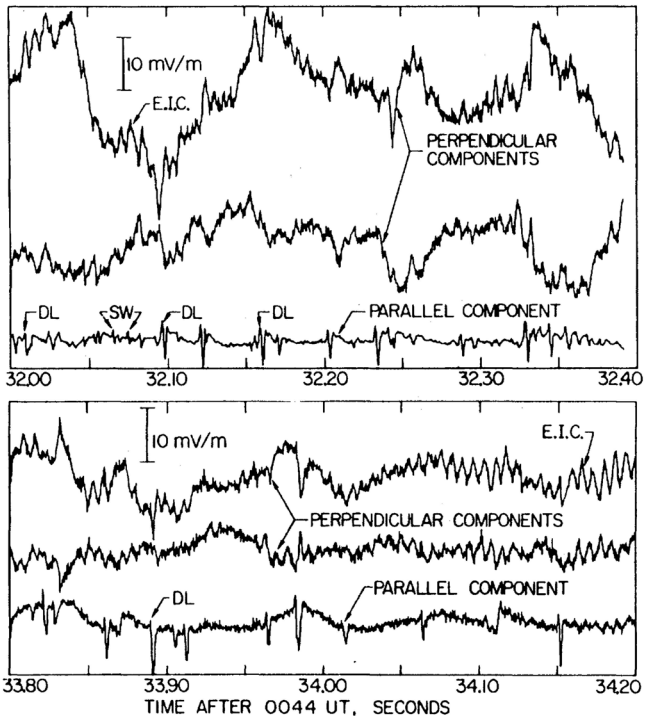

FIG. 3. Two perpendicular and one parallel electric field components in magnetic field-aligned coordinates for two events (top and bottom panels) that occurred 2 s apart. The data were acquired on August 11, 1976 when S3-3 was at an altitude of 6030 km, an invariant latitude of 74.1°, and a magnetic local time of 15.74 h. Examples of double layers (DLs), solitary waves (SWs), and electrostatic ion-cyclotron (EIC) waves are marked. Reprinted with permission from Temerin *et al.*, Phys. Rev. Lett. **48**, 1175 (1982). Copyright 1982 American Physical Society.[20]

up-going ion beams and enhanced loss-cones in ∼0.5 keV electrons. These particle signatures point toward the presence of 0.5 kV potential drops below the S3-3 spacecraft. The S3-3 observations of DL and SWs[20] were followed by the Viking observations by Boström *et al.*[21] and Koskinen *et al.*[22] The electrostatic solitary structures observed by S3-3 and Viking were interpreted as ion holes as they carried negative potentials and propagated along the magnetic field with speeds, ∼5 to ∼50 km s^{-1}, which are of the order of ion acoustic or ion beam speeds. The parallel electric field amplitudes were typically ∼15–20 mV m^{-1} with pulse durations of ∼2–20 ms. These earlier observations of solitary waves and double layers on the auroral field lines, coming from the analysis of waveform data, could not establish any link between the solitary waves and BEN as the data were not presented in the spectral form.

The first compelling observational breakthrough linking the observed solitary waves and BEN came from Geotail waveform capture data in the distant magnetotail. Matsumoto *et al.*[23] were the first to report the presence of solitary wave structures having positive potential in the plasma sheet boundary layer (PSBL) from the analysis of the Geotail Plasma Wave Instrument waveform data.

Figure 4 shows the frequency-time spectrogram of broadband electrostatic noise (BEN) observed in the PSBL at (–118 R_E, 4.3 R_E, 0.7 R_E) on April 1, 1993. The coordinates are in Geocentric solar magnetospheric (GSM) system. It is seen that intense BEN spectra extend all the way to the electron plasma frequency $f_{pe} \sim 2$ kHz. The bottom panel shows waveforms observed by the wave form capture (WFC) receiver at 13:55:43.241 UT. The observed waveforms, detected by the two orthogonally crossed set of electric field antennas, EU and EV, contain coherent structures with pulse widths of ∼2 ms. Matsumoto *et al.*[23] named these isolated pulse waveforms as electrostatic solitary waves (ESWs). Matsumoto *et al.*[23] showed that most of the BEN in the PSBL region is not continuous broadband noise but is composed of a series of ESWs in the form of a bipolar pulse, i.e., a half sinusoid-like cycle followed by a similar half cycle having opposite sign. They showed that the fast Fourier transform (FFT) of the bipolar pulses produces the observed BEN frequency spectra which has been reported by Scarf *et al.*[2] and Gurnett *et al.*[3] in the PSBL. Various earlier theories of BEN and its association with ESWs are reviewed by Lakhina *et al.*[18,25]

Since the geotail observations, similar ESWs have been observed in various regions of the Earth's magnetosphere and in the solar wind by many researchers using waveform data from FAST, Polar, WIND, Cluster, THEMIS, and Van Allen Probes spacecraft. For example, ESWs have been observed in the high-altitude polar magnetosphere, including the polar cap boundary layer (PCBL),[26–33] in the auroral acceleration region,[15,34–37] the magnetosheath,[10,38–40] the plasma sheet,[41] the reconnection regions at the dayside magnetopause,[42] the magnetotail,[43–46] the Earth's foreshock and

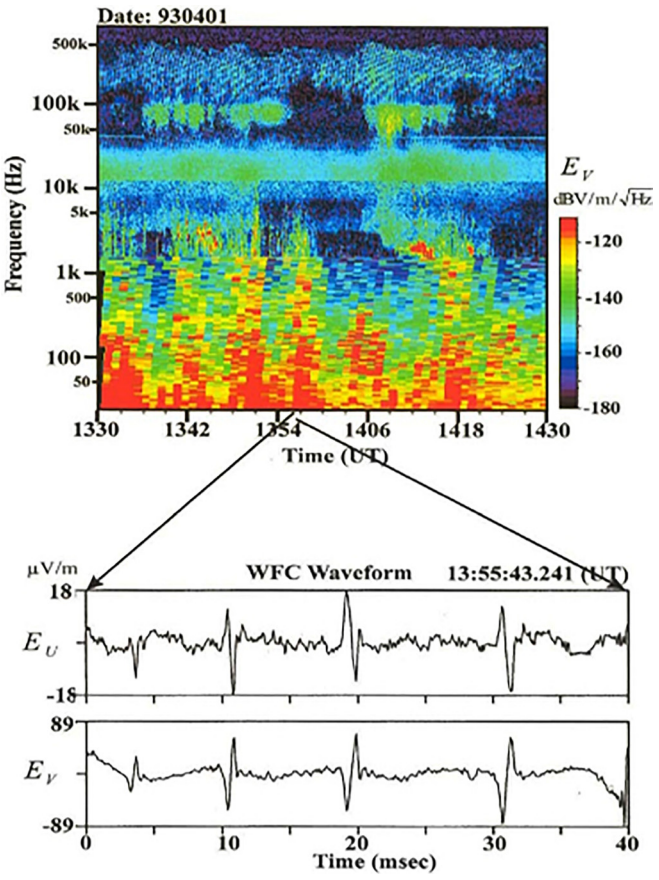

FIG. 4. Typical frequency-time spectrogram of the BEN in the plasma sheet boundary layer and the corresponding ESW waveforms in the time domain observed by GEOTAIL. Reprinted with permission from Kojima *et al.*, Adv. Space Res. **23**, 1689–1697 (1999). Copyright 1999 Elsevier.[24]

bow shock region,[47–49] the outer radiation belts,[50,51] the solar wind,[52,53] and the lunar wake.[54] The electrostatic solitary structures are found in the electric field parallel to the background magnetic field and are usually bipolar, sometimes monopolar or tripolar. The electrostatic solitary structures can have either negative (ion holes) or positive (electron holes) potentials, and their electric field amplitudes decrease with distance from the Earth, i.e., from $\sim$100 mV m^{-1} in the auroral region to fraction of a mV m^{-1} in the PSBL and magnetosheath regions.[15,23,35,38,40,55–57] However, the velocities and parallel scale sizes of ESWs are generally found to increase with the distance from the Earth. For example, the field-aligned velocities of ESWs may vary from $\sim$a few 100s km s^{-1} to a few 10 000s km s^{-1}, and their parallel scale sizes can vary from $\sim$100 m to tens of kilometer, as one goes from the auroral region to the plasma sheet boundary layer.[29,55] The ESWs are roughly of spherical shape when $R = f_{ce}/f_{pe} > 1$, and their shapes become more oblate (with the perpendicular scale larger than the parallel scale) as R decreases to less than 1.[58] Here, f_{ce} and f_{pe} are the electron cyclotron frequency and the electron plasma frequency, respectively. Further, generally the ESWs observed by spacecraft are characterized by an amplitude-width relationship where the amplitude of the electrostatic potential of the solitary wave tends to increase with its width.[35,40,56]

II. MODELS FOR THE ESWs

The ESWs are found in different regions of the magnetosphere and in the solar wind. The ESWs are responsible for the broadband electrostatic noise (BEN) or the electrostatic turbulence observed in the magnetosphere and solar wind, and they may also affect the efficiency of magnetic reconnection process. The ESWs observed in various regions seem to have some common physical mechanisms involving electron or ion beams or nonthermal distributions of electrons or ions. Various models have been proposed to explain the solitary pulses [for a review, see Ref. 18]. All models fall basically into two categories, namely, BGK modes/phase space holes and solitons/solitary waves.

A. BGK modes/phase space holes

The most popular interpretations for the electrostatic solitary waves (ESWs) observed in the magnetosphere are in terms of Bernstein-Green-Kruskal (BGK) modes or phase space holes,[59–62] where the trapped particle population plays a crucial role. The electron holes and ion holes have been proposed for the positive and negative potential solitary structures, respectively.[35,38,40,56,63–68] Matsumoto *et al.*[23] and Omura *et al.*[69] were able to successfully reproduce the waveforms of ESWs observed by Geotail from simulations of electron beam-plasma system employing one-dimensional electrostatic particle codes. Their results clearly showed that nonlinear evolution of electron beam instabilities leads to the formation of isolated stable electrostatic potential structures, equivalent to Bernstein-Green-Kruskal (BGK) modes[59] propagating along the magnetic field. They hypothesized that the ESWs were the BGK mode electron phase-space holes or simply electron holes (EHs). An excellent review of electron phase space holes is given by Hutchinson.[70] Based on kinetic simulations, Goldman *et al.*[64] and Oppenheim *et al.*[65] have given an explanation for the bipolar structures observed by FAST on the auroral field lines[15,35] in terms of nonlinear two-stream instabilities,[71–74] a mechanism similar to that of PSBL BEN proposed by Omura *et al.*[63] and Kojima *et al.*[38] However, the phase space holes observed in these simulations are not stable, and they are likely to either merge or breakup during the evolution of the instability. The electron magnetization plays an important role on the shape and stability of the phase space holes.[75] Singh *et al.*[73] carried out 3D particle simulation of electron holes (e-holes) and found that e-holes are essentially planar and highly transitory for $R < 1$, while for $R \geq 2$, they are long lasting and can have a variety of structures from spherical to planar, which is consistent with the observations of ESWs by Franz *et al.*[58]

In a series of papers, Jovanović and colleagues have discussed the theory of ion and electron holes in magnetized plasmas. For electron holes, they employ the drift kinetic description for electrons and treat the ions as either weakly magnetized or unmagnetized. The stationary solution of Vlasov-Poisson equation yields quasi 3-D electron holes which generally have the form of a cylinder that is tilted relative to the magnetic field or spheroids.[76–81] These electron hole models may provide a theoretical explanation for the positive potential ESWs having bipolar spikes in the parallel electric field. On the other hand, for the ion holes, Jovanović *et al.* consider the drift kinetic description for the ions and treat electrons either hydrodynamically or as having Boltzmann distribution. The stationary solution of Vlasov-Poisson equations yields quasi 2-D or 3-D ion holes in the form of either cylinders or spheroids.[82,83] Such ion holes may explain the properties of negative potential ESWs having bipolar spikes in the parallel electric field as observed on the auroral field lines.

Jovanović *et al.*[84] have constructed a self-consistent, stationary nonlinear solution of the one-dimensional Vlasov–Poisson equations in an unmagnetized plasma, which describes a coupled ion and electron hole pair. This model may provide a theoretical explanation for the tripolar electric field pulses observed by Cluster[85] and WIND[52] spacecrafts.

Jovanović and Krasnoselskikh[86] have developed a nonlinear kinetic theory for ion humps at the foot of the Earth's bow shock. In this model, ions are unmagnetized and have two populations, namely, stationary (i.e., solar wind) ions and back-streaming (i.e., bow shock reflected) ions, and electrons are taken as weakly magnetized. These coherent structures may provide a theoretical explanation for the bipolar electric pulses observed upstream of the shock by Polar[87] and Cluster spacecraft.[88]

B. Solitons/solitary waves

As stated earlier, the amplitudes of the electrostatic potential of ESWs observed by spacecraft are usually found to increase with their widths. This property of ESWs is opposite to that of KdV (Korteweg-de Vries) type solitons where the soliton amplitude increases as its width decreases. This clearly shows that the ESWs observed by spacecraft are not the usual KdV type of small-amplitude ion-acoustic or electron-acoustic solitons. There has been a misconception prevailing in the space plasma community that all weak

solitons should behave like KdV solitons. Because of this misconception, the generation mechanisms for ESWs based on ion-acoustic or electron-acoustic solitons were considered unfeasible.[35,40,56] The properties of the arbitrary amplitude ion- and electron-acoustic solitons predicted by the models based on the Sagdeev pseudo-potential[89] techniques are quite different from the KdV type solitons. These models show that depending upon the parametric range, the soliton amplitudes can either increase or decrease with the increase in their width.[90] This has brought the soliton/double layer models based on Sagdeev pseudo-potential method to the forefront of viable models for the generations of ESWs. In particular, the models based on arbitrary amplitude electron-acoustic solitary waves[91–100] are being considered as an alternative to the phase-space electron holes models[38,57,63,64,66–68,101,102] for the generation of ESWs.

1. Current status of soliton models

Ion-acoustic solitons and double layers have been suggested to explain the properties of ESWs observed on the auroral field lines by S3-3[20] and Viking[21,22] by several researchers.[103–109] Electron-acoustic solitons have been proposed to explain the negative potential ESWs observed by Viking.[13,14,91,92,110–113] However, none of these models could explain the positive potential solitary structures observed by Polar, FAST, and Cluster. Berthomier *et al.*[114,115] showed that in the presence of an electron beam, one can get electron-acoustic solitons with positive polarity in a certain parametric regime. For a detailed discussion of earlier models, one can refer to Lakhina *et al.*[18,116] Verheest *et al.*[117] and Cattaert *et al.*[118] showed that, even in the absence of an electron beam, both positive and negative potential electron-acoustic solitons can exist in a two temperature electron plasma system, provided the hot electron inertia is retained in the analysis. Singh *et al.*[119] showed that the inertia of the warm electrons, and not the electron beam speed, is essential for the generation of positive potential solitary structures.

In a series of papers, Lakhina and colleagues[95–99] have developed multi-fluid models, with no restriction on the number of species or their drift speeds, to study arbitrary amplitude ion- and electron-acoustic solitons and double layers. These models consider the inertia of all species and employ Sagdeev pseudo-potential technique and are valid for parallel propagating nonlinear structures. For example, the model for ion- and electron-acoustic solitons and double layers in a four-component plasma system consisting of core electrons, two counter-streaming electron beams, and one type of ions[97] has been applied to the ESWs observed by Cluster spacecraft in the magnetosheath.[10] When the actual plasma parameters corresponding to ESWs were put into this model, only one positive critical Mach number, M_0, apparently related to fast electron acoustic beam mode was found, which yielded soliton and/or double layer solution. The estimates of the electric field, pulse duration, and propagation speeds of the solitary structures predicted by the model were in good agreement with the observed bipolar pulses. Lakhina *et al.*[99] have shown that a similar model can explain the generation of broadband (~2–6 kHz) electrostatic noise observed by Cluster spacecraft in the plasma sheet boundary layer in association with cold counter-steaming electron beams flowing through the hot Maxwellian plasma[120] in terms of electron-acoustic solitons and double layers. For the plasma parameters at the time of broadband electrostatic noise observed by Cluster on September 22, 2004,[120] the model predicts solitons/double layer with electric field ~(0.01–30) mV m^{-1} with time durations ~(0.1–4.5) ms. Such short electric field pulses, when Fourier transformed to the frequency domain, can appear as broadband electrostatic noise in the frequency range of ~220 Hz to 10 kHz. This model[99] seems to be a good candidate for explaining the generation of broadband electrostatic noise in the plasma sheet boundary layer.

The pioneer work on ion-acoustic solitons was started about 50 years ago by Sagdeev[89] and Washimi and Taniuti.[121] Observations of solitary waves and double layers by S3-3, Viking, Polar, FAST, and other spacecrafts gave a spurt to the theoretical studies of ion-acoustic solitons and double layers,[90,95,96,98,99,103,107–109,122–137] and electron-acoustic solitons and double layers[13,91–96,100,111–115,118,119,137–146] in multi-component unmagnetized, as well as in magnetized plasmas. In these studies, various plasma species were treated either as fluids or having Maxwellian particle distributions. However, space plasmas are often found to have non-Maxwellian particle distribution functions that contain suprathermal particles having high-energy tails.[147–150] The suprathermal electron (or ion) component may result from an acceleration mechanism by wave-particle interaction in the presence of plasma turbulence, e.g., lower hybrid, Alfvén, or some other plasma waves.[151] The kappa distribution has been widely adopted to model the observed suprathermal particle distributions.[152–163]

There are several studies dealing with the ion-acoustic or/and electron-acoustic solitary waves with highly energetic kappa-distributed electrons.[164–174] In this review, we shall discuss the fluid models for the ion- and electron-acoustic solitons and double layers in multi-component space plasmas where the hot electrons are characterised by kappa distributions. We shall then discuss two specific applications of these models pertaining to the observations of (1) coherent low-frequency electrostatic waves and weak double layers in the solar wind and (2) ESWs and electrostatic waves in the lunar wake.

III. FLUID MODELS FOR ION-AND ELECTRON-ACOUSTIC SOLITONS AND DOUBLE LAYERS IN MULTI-COMPONENT PLASMAS

A most general theoretical model for the solar wind/lunar wake plasma is considered.[170,173,174] The four-component plasma is assumed as a homogeneous, collisionless, and magnetized comprising of protons (N_{p0}, T_p), heavier ions, i.e., alpha particles, He^{++} (N_{i0}, T_i, U_i), electron beam (N_{b0}, T_b, V_b), and suprathermal electrons (N_{e0}, T_e). Here, N_{j0} and T_j represent the equilibrium densities and temperatures of the jth species, where j = p, i, b, and e for protons, heavier ions, electron beam, and suprathermal electrons, respectively, and U_i and V_b are the ion and electron beam speeds parallel to the ambient magnetic field, $\mathbf{B}_0$.

The suprathermal electrons in the solar wind/lunar wake follow the κ-distribution given by Summers and Thorne[152]

$$f_e(\nu) = \frac{N_{e0}}{\sqrt{\pi}\theta}\frac{\Gamma(\kappa)}{\sqrt{\kappa}\,\Gamma(\kappa-1/2)}\left(1+\frac{\nu^2}{\kappa\theta^2}\right)^{-\kappa}. \quad (1)$$

Here, $\Gamma(\kappa)$ is the gamma function, and κ is the spectral index and is a measure of the proportion of high-energy particles present in the distribution. The κ-distribution given by Eq. (1) is properly defined for $\kappa > 3/2$. In space plasmas, typically κ is found to be in the range of $2 < \kappa < 6$. Furthermore, when $\kappa \to \infty$, the κ-distribution approaches a standard Maxwellian distribution. The modified electron thermal speed, θ, is given by

$$\theta = \sqrt{\left(2-\frac{3}{\kappa}\right)\frac{T_e}{m_e}}.$$

Here, T_e and m_e are the electron temperature and mass, respectively. The electrostatic solitons are considered to be propagating parallel to the ambient magnetic field. The number density of the suprathermal electrons which are described by κ distribution can be obtained by replacing $\frac{v^2}{\theta^2}$ by $\frac{v^2}{\theta^2}-\frac{2e\phi}{m\theta^2}$ in Eq. (1) and integrating it over the velocity space and is given by[166]

$$n_e = n_{e0}\left(1-\frac{\phi}{\kappa-3/2}\right)^{-\kappa+1/2}. \quad (2)$$

On the other hand, the dynamics of protons, heavier ions, and electron-beam in the solar wind/lunar wake plasma is governed by the following multi-fluid equations in the normalized form:

$$\frac{\partial n_j}{\partial t}+\frac{\partial(n_j v_j)}{\partial x}=0, \quad (3)$$

$$\frac{\partial v_j}{\partial t}+v_j\frac{\partial v_j}{\partial x}+Z_j\mu_{pj}\frac{\partial\phi}{\partial x}+3\mu_{pj}\sigma_j\frac{n_j}{n_{j0}^2}\frac{\partial n_j}{\partial x}=0, \quad (4)$$

$$\frac{\partial^2\phi}{\partial x^2}=(n_e+n_b-n_p-Z_i n_i). \quad (5)$$

It may be noted that Eq. (4) combines both the momentum equation and equation of state and the adiabatic index $\gamma_j = 3$, and Eqs. (2)–(5) are the normalized set of equations. Here, the number densities are normalized by the total equilibrium number density of electrons (protons), $N_0 = N_{p0} + Z_i N_{i0} = N_{e0} + N_{b0}$, and the velocities are normalized with the ion-acoustic speed, $C_a = \sqrt{T_e/m_p}$; m_p is the mass of the proton, lengths are normalized with the effective hot electron Debye length, $\lambda_{de} = \sqrt{T_e/4\pi N_0 e^2}$; e is the electronic charge, time is normalized with the inverse of the effective proton plasma frequency, $f_{pp} = \sqrt{4\pi N_0 e^2/m_p}$, and the electrostatic potential ϕ is normalized with T_e/e. Further, $\mu_{pj} = m_p/m_j$, where m_j is the mass of the jth species. Similarly, $\sigma_j = T_j/T_e$ and $n_{j0} = N_{j0}/N_0$ are the normalized temperature and equilibrium number density of jth species and v_j is the normalized fluid velocity. Also, $Z_j = +1$ for protons, $Z_j = +2$ for heavier ions (alpha particles), and $Z_j = -1$ for beam electrons.

In order to study the properties of large amplitude electrostatic solitons, the set of Eqs. (2)–(5) is transformed into a stationary frame moving with phase velocity, V of the electrostatic solitary wave, i.e., $\xi = x - Mt$, where $M = V/C_a$ is the Mach number. Furthermore, the perturbed number densities of protons, heavier ions, electron-beam, and suprathermal electrons are obtained by solving Eqs. (2)–(5). These number densities are substituted in the Poisson equation (5), and we obtain an energy integral after assuming appropriate boundary conditions for the localized disturbances along with the conditions that electrostatic potential $\phi = 0$, and $d\phi/d\xi = 0$ at $\xi \to \pm\infty$. The energy integral is given by

$$\frac{1}{2}\left(\frac{d\phi}{d\xi}\right)^2+S(\phi,M)=0. \quad (6)$$

Equation (6) describes the motion of a pseudo-particle of unit mass in a pseudopotential $S(\phi, M)$, where, ϕ and ξ play the role of displacement from the equilibrium and time, respectively. The Sagdeev pseudopotential, $S(\phi, M)$, is given by[173,174]

$$\begin{aligned}S(\phi,M) = {} & \frac{n_{p0}}{6\sqrt{3\sigma_p}}\left\{\left(M+\sqrt{3\sigma_p}\right)^3-\left[\left(M+\sqrt{3\sigma_P}\right)^2-2\phi\right]^{3/2}-\left(M-\sqrt{3\sigma_p}\right)^3+\left[\left(M-\sqrt{3\sigma_p}\right)^2-2\phi\right]^{3/2}\right\}\\ & +\frac{n_{i0}}{6\sqrt{3\sigma_i}}\left\{\left(\frac{M-U_0}{\sqrt{\mu_{pi}}}+\sqrt{3\sigma_i}\right)^3-\left[\left(\frac{M-U_0}{\sqrt{\mu_{pi}}}+\sqrt{3\sigma_i}\right)^2-2Z_i\phi\right]^{3/2}-\left(\frac{M-U_0}{\sqrt{\mu_{pi}}}-\sqrt{3\sigma_i}\right)^3\right.\\ & \left.+\left[\left(\frac{M-U_0}{\sqrt{\mu_{pi}}}-\sqrt{3\sigma_i}\right)^2-2Z_i\phi\right]^{3/2}\right\}+\frac{n_{b0}}{6\sqrt{3\sigma_b}}\left\{\left(\frac{M-V_{b0}}{\sqrt{\mu_{pe}}}+\sqrt{3\sigma_b}\right)^3-\left[\left(\frac{M-V_{b0}}{\sqrt{\mu_{pe}}}+\sqrt{3\sigma_b}\right)^2+2\phi\right]^{3/2}\right.\\ & \left.+\left[\left(\frac{M-V_{b0}}{\sqrt{\mu_{pe}}}-\sqrt{3\sigma_b}\right)^2+2\phi\right]^{3/2}-\left(\frac{M-V_{b0}}{\sqrt{\mu_{pe}}}-\sqrt{3\sigma_b}\right)^3\right\}+n_{e0}\left[1-\left(1-\frac{\phi}{\kappa-3/2}\right)^{-\kappa+3/2}\right]. \quad (7)\end{aligned}$$

Note that Eq. (7) is written in the symbolic form where the operation of a square root on a squared expression returns the same expression, e.g., $\sqrt{(M\pm\sigma_j)^2} = M\pm\sigma_j$. Here, $U_0 = U_i/C_a$ and $V_{b0} = V_b/C_a$. Note that in the absence of beam electrons, the results of Lakhina and Singh[170] can be recovered. On the other hand, in the absence of beam electrons and ion streaming, the results of Rubia *et al.*[171] can be obtained.

For the existence of soliton solutions, the Sagdeev pseudopotential $S(\phi, M)$ must satisfy the following conditions: (i) $S(\phi, M) = 0$, $dS(\phi, M)/d\phi = 0$, and $d^2S(\phi, M)/d\phi^2 < 0$ at $\phi = 0$, (ii) $S(\phi, M) = 0$ at $\phi = \phi_{max}$ (ϕ_{max} is the maximum attainable amplitude of the soliton), and (iii) $S(\phi, M) < 0$ for $0 < |\phi| < |\phi_{max}|$. Further, for a double layer solution, in addition to the soliton conditions (i)–(iii), the condition (iv) $dS(\phi, M)/d\phi = 0$ at $\phi = \phi_{max}$ has to be satisfied.

The Sagdeev pseudopotential, $S(\phi, M)$, given in Eq. (7) and its first derivative with respect to ϕ vanish at $\phi = 0$. The soliton condition $d^2S(\phi, M)/d\phi^2 < 0$ at $\phi = 0$ is satisfied, provided $M > M_0$, where M_0 is the critical Mach number which satisfies the following equation:

$$\frac{n_{p0}}{M^2-3\sigma_p}+\frac{n_{i0}Z_i^2}{\dfrac{(M-U_0)^2}{\mu_{pi}}-3\sigma_i}+\frac{n_{b0}}{\dfrac{(M-V_{b0})^2}{\mu_{pe}}-3\sigma_b}=n_{e0}\left(\frac{2\kappa-1}{2\kappa-3}\right). \tag{8}$$

The critical Mach number, M_0, is obtained by numerically solving Eq. (8). It is evident from Eq. (8) that it will have six roots but all roots may not be physical. Therefore, we consider only real positive roots for M_0 and Eq. (8) yields three positive roots for relevant solar wind/lunar wake plasma parameters. The smallest, intermediate, and largest roots are corresponding to the slow ion-acoustic, fast ion-acoustic, and electron-acoustic modes, respectively. The fast ion-acoustic mode is similar to the ion-acoustic mode of proton-electron plasma, whereas slow ion-acoustic mode is a new mode that occurs due to the presence of heavier ions. It is also known as ion-ion hybrid mode that requires two ion species having different thermal velocities or a relative streaming between the ions.[170]

It is important to point out that the third derivative of the Sagdeev pseudopotential, $S(\phi, M)$, evaluated at $\phi = 0$, essentially provides the polarity of the solitons. Therefore, the positive (negative) values of Eq. (9) evaluated at $M = M_0$ correspond to electrostatic solitons having positive (negative) electrostatic potential, ϕ.[100,127,171] Further, whenever the solitons are found to have finite amplitude at $M = M_0$, the coexistence of both polarity solitons is feasible[175]

$$\left(\frac{d^3S(\phi,M)}{d\phi^3}\right)_{\phi=0}=\frac{3n_{p0}(M^2+\sigma_p)}{(M^2-3\sigma_p)^3}+\frac{3n_{i0}Z_i^3\left(\dfrac{(M-U_0)^2}{\mu_{pi}}+\sigma_i\right)}{\left(\dfrac{(M-U_0)^2}{\mu_{pi}}-3\sigma_i\right)^3}-\frac{3n_{b0}\left[\dfrac{(M-V_{b0})^2}{\mu_{pe}}+\sigma_b\right]}{\left[\dfrac{(M-V_{bo})^2}{\mu_{pe}}-3\sigma_b\right]^3}-n_{e0}\frac{(4\kappa^2-1)}{(2\kappa-3)^2}. \tag{9}$$

A. Three component model for ion-acoustic solitons and double layers in the solar wind

As a special case, we neglect the electron beam in the above analysis. Then, the remaining three components, namely,

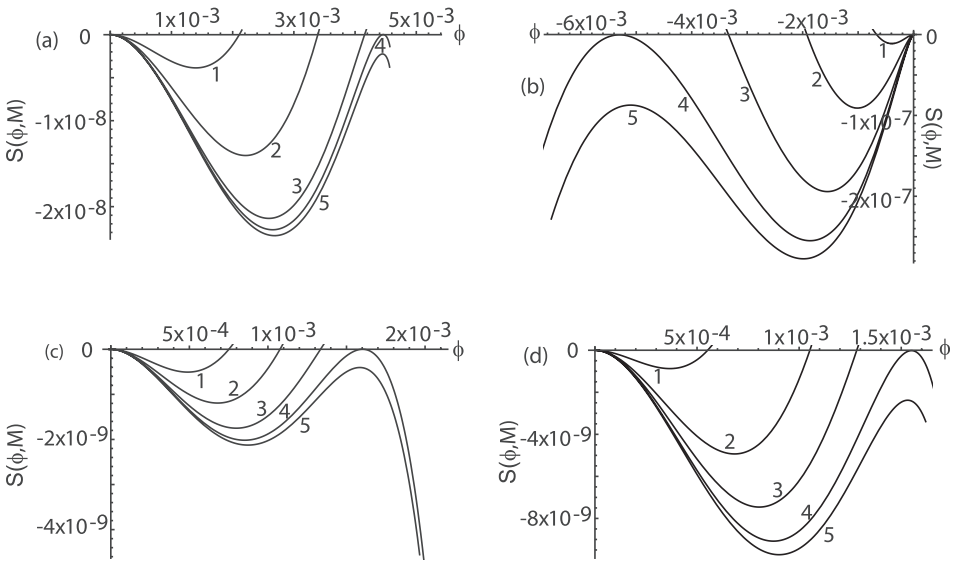

FIG. 5. Sagdeev pseudopotential $S(\phi, M)$ *versus* the potential ϕ for the slow ion-acoustic solitons and double layer. The normalized parameters are in (a) $N_i = 0.01$, $T_p = 1.0$, $T_i/T_p = 4.0$, $U_0 = 0.3$, $\kappa = 10$, $M = 1.963$, 1.964, 1.9644, 1.96446 (DL), and 1.96449 for the curves 1, 2, 3, 4, and 5, respectively; in (b) $N_i = 0.05$, $T_p = 2.0$, $T_i/T_p = 2.0$, $U_0 = 0.8$, $\kappa = 5$, $M = 2.525$, 2.529, 2.531, 2.5317635 (DL), and 2.532 for the curves 1, 2, 3, 4, and 5, respectively; in (c) $N_i = 0.05$, $T_p = 0.2$, $T_i/T_p = 4.0$, $U_0 = 0.2$, $\kappa = 2$, $M = 0.9214$, 0.9215, 0.92155, 0.921569 (DL), and 0.921576 for the curves 1, 2, 3, 4, and 5, respectively; in (d) $N_i = 0.05$, $T_p = 0.5$, $T_i/T_p = 2.0$, $U_0 = 0.5$, $\kappa = 2$, $M = 1.322$, 1.3225, 1.32265, 1.322724 (DL), and 1.32275 for the curves 1, 2, 3, 4, and 5, respectively. Reprinted with permission from Lakhina and Singh, Sol. Phys. **290**, 3033–3049 (2015). Copyright 2015 Springer Nature.[170]

the protons, streaming α particles, and suprathermal electrons having a κ distribution, can model the solar wind plasma quite well.[170] On putting $n_{b0} = 0$ in Eq. (8), the soliton condition for critical Mach number $M = M_0$ becomes

$$\frac{n_{p0}}{M_0^2 - 3\sigma_p} + \frac{n_{i0}Z_i^2}{\frac{(M_0 - U_0)^2}{\mu_{pi}} - 3\sigma_i} = n_{e0}\left(\frac{2\kappa - 1}{2\kappa - 3}\right). \quad (10)$$

In the absence of heavier ions ($n_{i0} = 0$), Eq. (10) has a single positive root, namely,

$$M_0^2 = \left[\frac{\kappa - 3/2}{\kappa - 1/2} + 3\sigma_p\right], \quad (11)$$

which describes the ion-acoustic mode in a plasma with κ distributed electrons and hot protons. However, when heavier ions are present, Eq. (10) predicts another mode having lower values of M_0 as discussed by Lakhina and Singh.[170] We will refer to the root of Eq. (10) with higher values as the fast ion-acoustic mode and to the root with lower M_0 values as the slow ion-acoustic mode.[96,170,176] From Eq. (10), we note that when $U_0 = 0$ and $T_i/T_p = m_i/m_p$, we get only the fast ion-acoustic mode similar to that given by Eq. (11) but modified in the presence of the heavier ions. However, for $U_0 \neq 0$, the slow ion-acoustic mode can always exist in the solar wind. An interesting property of the new slow ion-acoustic mode is that it can support positive/negative potential solitons/double layers depending on the plasma parameters.[170,176]

1. Numerical results

We use the normalized parameter dataset which is based on various solar wind observations. For the fast solar wind, we take the proton to electron temperature ratio, $T_p/T_e \geq 1$, α to electron density ratio, $N_i/N_e = 0.0 - 0.05$; α to proton temperature ratio, $T_i/T_p \geq 1$; ratio of relative drift between α particles and protons and ion-acoustic speed, $U_0 = 0.0 - 2.0$. Whereas for the slow solar wind, we consider $T_p/T_e < 1$, $N_i/N_e = 0.0 - 0.05$, $T_i/T_p \geq 1$ and $U_0 = 0.0 - 0.3$ [considering a relative drift between αs and protons of ∼0–10 km s^{-1} and ion-acoustic speed of ∼35 km s^{-1}].[52,177,178] Furthermore, we shall consider the κ index for electrons to vary from 2 to 10 to cover the range of values observed in the solar wind.[162,179] We use these datasets in Eq. (10) and find the critical Mach numbers, M_0, by solving this equation numerically.

Figure 5 shows the variation of the Sagdeev potential $S(\phi, M)$ *versus* the normalized electrostatic potential ϕ for various values of the Mach number in the case of the slow ion-acoustic mode. Four cases of double layer occurrence under different solar wind conditions are shown. Panels (a) and (b) correspond to typical conditions occurring during the fast solar wind, whereas panels (c) and (d) correspond to the slow and intermediate solar wind conditions, respectively. A look at the different curves in panels (a)–(d) shows that the slow ion-acoustic soliton amplitude increases with M (cf. curves 1, 2, and 3) till a double layer (curve 4) is formed. Solitons do not exist for Mach numbers greater than the double-layer Mach number (cf. curve 5). Therefore, the double layers provide the upper limit on the Mach number, M_{max}. Panels (a), (c), and (d) show the examples of positively charged (i.e., $\phi > 0$) solitons and double layers, whereas panel (b) shows negatively charged (with $\phi < 0$) solitons and a double layer.

Figure 6 shows the variation of the Sagdeev potential $S(\phi, M)$ *versus* the normalized electrostatic potential ϕ for various values of the Mach number in the case of the fast ion-acoustic mode, under the same parameters as in Fig. 5. It is evident that fast ion-acoustic solitons occur for higher values of M as compared to those shown in Fig. 5. Here, also the soliton amplitude increases with M till the upper limit of curve 4 is reached (cf. curves 1, 2, 3, and 4) and beyond that the soliton solution does not exist. Since the double layers do not occur, the upper limit M_{max} on the Mach numbers is provided by the restriction that the heavier ion number density be real.[127] Hence, the solitons/double layers for both slow and fast ion-acoustic modes occur in a Mach number region $M_0 < M \leq M_{max}$.

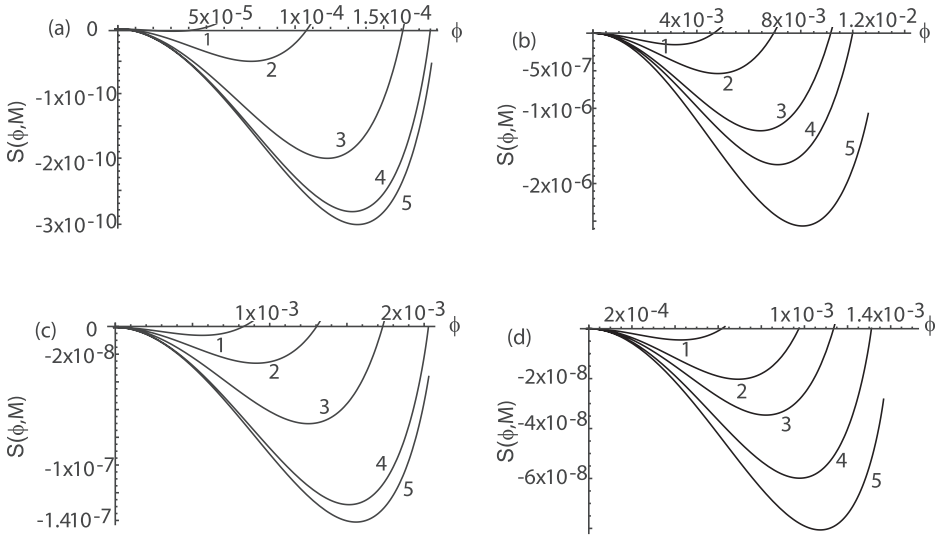

FIG. 6. Sagdeev pseudopotential $S(\phi, M)$ *versus* the potential ϕ for the fast ion-acoustic solitons for same plasma parameters as in Fig. 5 except that Mach numbers are different in each panel. The parameters are for panel (a): $M = 2.043$, 2.044, 2.045, 2.04533, and 2.0454 for the curves 1, 2, 3, 4, and 5, respectively; panel (b): $M = 2.62$, 2.625, 2.63, 2.63205, and 2.635 for the curves 1, 2, 3, 4, and 5, respectively; panel (c): $M = 1.014$, 1.016, 1.018, 1.01962, and 1.0199 for the curves 1, 2, 3, 4, and 5, respectively; panel (d): $M = 1.398$, 1.40, 1.401, 1.40223, and 1.403 for the curves 1, 2, 3, 4, and 5, respectively. Reprinted with permission from Lakhina and Singh, Sol. Phys. **290**, 3033–3049 (2015). Copyright 2015 Springer Nature.[170]

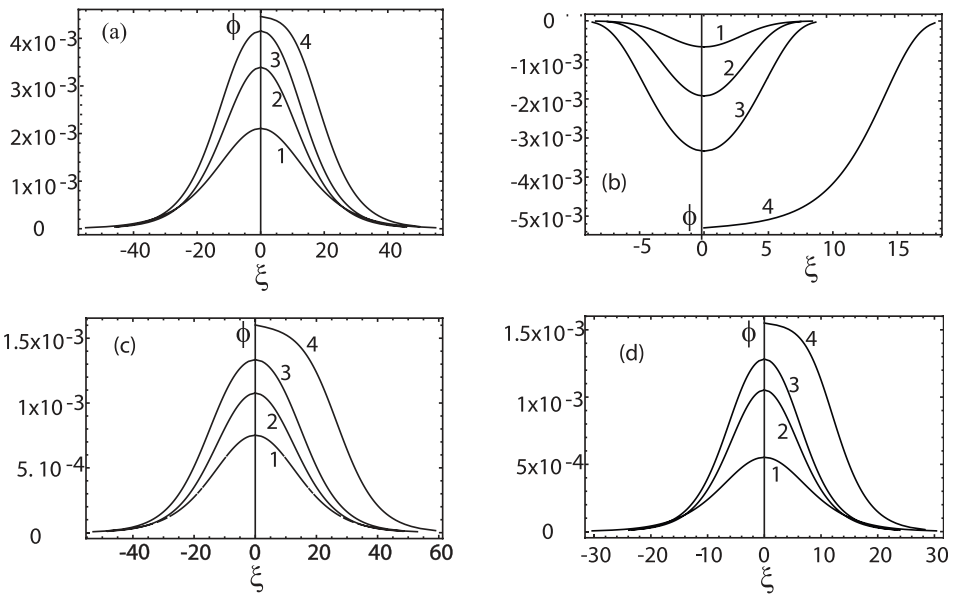

FIG. 7. Potential ϕ profiles for the slow ion-acoustic solitons and double layers for the plasma parameters of Fig. 5. The curves 1, 2, 3, and 4 in each panel corresponds to the Mach numbers in the corresponding panel in Fig. 5. The profiles shown in panels (a), (c), and (d) are for the positive potential solitons (curves 1, 2, and 3) and a double layer (curve 4). The profiles shown in panel (b) are for the negative potential solitons (curves 1, 2, and 3) and a DL (curve 4). Reprinted with permission from Lakhina and Singh, Sol. Phys. **290**, 3033–3049 (2015). Copyright 2015 Springer Nature.[170]

Figure 7 shows profiles of the potential ϕ for slow ion-acoustic solitons and double layer for the solar wind plasma parameters of Fig. 5. The curves 1, 2, 3, and 4 in each panel correspond to the Mach number in the corresponding panel in Fig. 5. It is seen that solitons [cf. curves 1, 2, and 3 in panels (a)–(d)] have symmetric profiles and double layers [cf. curve 4 in panels (a)–(d)] have asymmetric profiles. Defining the soliton/DL width, W, as the full width at half maximum, we get the soliton/DL widths as W = 32.0, 28.0, 30.0, and 20.0 for panel (a); W = 7.5, 8.0, 10.0, and 13.0 for panel (b); W = 32.5, 32.5, 34, and 27.5 for panel (c), and W = 19.0, 18.0, 19.0, and 12.0 for panel (d). All these correspond to curves 1, 2, 3, and 4 in each panel, respectively.

Figure 8 shows the electric field, E, profiles for the slow ion-acoustic solitons and double layers corresponding to Fig. 7. The curves 1, 2, and 3 are for the solitons, and the curve 4 are for the double layers. The electric fields for the solitons have bipolar structures, whereas those for the DLs have monopolar structures. Furthermore, the largest and the smallest electric fields for solitons and double layers occur in panels (b) and (c), respectively.

B. Four component model for ion- and electron-acoustic soliton in the lunar wake

In this second special case, we neglect the streaming of the ions. Thus, the four component model comprising of protons, α particles, and suprathermal electrons having a κ distribution and electron beam is relevant to lunar wake as discussed in Ref. 173. Therefore, with $U_0 = 0$ in Eq. (8), the critical Mach number $M = M_0$ for solitons can be obtained from the following equation:

$$\frac{n_{p0}}{M^2 - 3\sigma_p} + \frac{n_{i0}Z_i^2}{\frac{M^2}{\mu_{pi}} - 3\sigma_i} + \frac{n_{b0}}{\frac{(M - V_{b0})^2}{\mu_{pe}} - 3\sigma_b} = n_{e0}\left(\frac{2\kappa - 1}{2\kappa - 3}\right). \tag{12}$$

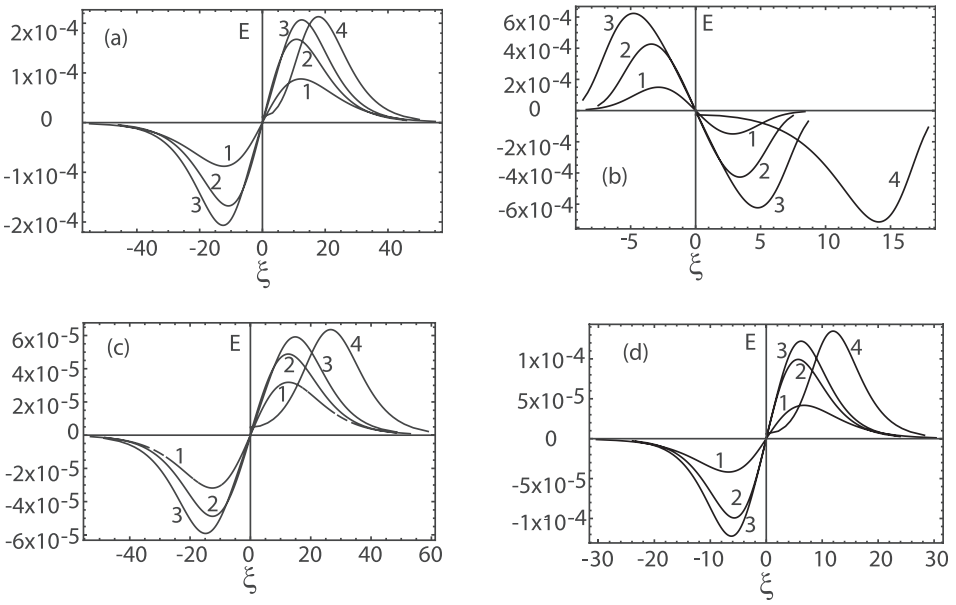

FIG. 8. Electric field E profiles for the slow ion-acoustic solitons and double layers for the plasma parameters of Fig. 5. The curves 1, 2, 3, and 4 in each panel correspond to the Mach numbers in the corresponding panel in Fig. 5. The electric field profiles of the solitons have bipolar structures [cf. curves 1, 2, and 3 in panels (a)–(d)] and those of the double layers have a monopolar structures [cf. curve 4 in panels (a)–(d)]. Reprinted with permission from Lakhina and Singh, Sol. Phys. **290**, 3033–3049 (2015). Copyright 2015 Springer Nature.[170]

Equation (12) will have six roots for the relevant lunar wake plasma parameters. As has been described under Eq. (8) in Sec. III, the smallest and intermediate roots correspond to the slow and fast ion-acoustic modes, respectively, and the largest root corresponds to the electron-acoustic mode.[96,170,173,174,176]

1. Numerical results

For the lunar wake plasma parameters, Eq. (7) with $U_0 = 0$ is solved numerically for the Sagdeev pseudopotential, $S(\phi, M)$. The exact parameters of the two runs, i.e., run 1 and run 2 as given by Tao *et al.*,[180] are considered. They are first converted to the normalized values and then used as input for the model. For the numerical computations, the following normalized parameters are considered: run 1—$\kappa = 6$, $n_{b0} = 0.01$, $\sigma_b = 0.0025$, and $V_{b0} = 17.14$ and run 2—$\kappa = 6$, $n_{b0} = 0.015$, $\sigma_b = 0.01$, and $V_{b0} = 17.14$. It must be emphasized here that the solar wind plasma parameters are used for number density, temperature of heavier ions, and the temperature of protons as these were not provided in Ref. 180. Hence, slow solar wind parameters[52,170] used in the calculations are $n_{i0} = 0.05$, $\sigma_p = 0.2$, and $\sigma_i = 0.4$. This is justified that it is the solar wind plasma that refills the lunar wake through ambipolar diffusion. Further, all the three modes, i.e., slow and fast ion-acoustic mode as well as electron-acoustic mode are observed for run 1 and run 2 parameters.

For run 1 parameters, $n_{i0} = 0.05$, $n_{b0} = 0.01$, $\sigma_p = 0.2$, $\sigma_i = 0.4$, $\sigma_b = 0.0025$, and $\kappa = 6$, panel (a) in Fig. 9 shows the Sagdeev potential $S(\phi, M)$ versus the normalized electrostatic potential ϕ for various values of the Mach number for the slow ion-acoustic solitons. The slow ion acoustic solitons supports only positive polarity solitons which is consistent with the sign of the third derivative of the Sagdeev potential evaluated at $M = M_0$, as given by Eq. (9). The upper limit M_{max} on the Mach number for which soliton solutions exist is provided by the restriction that the heavier ion density, n_i,

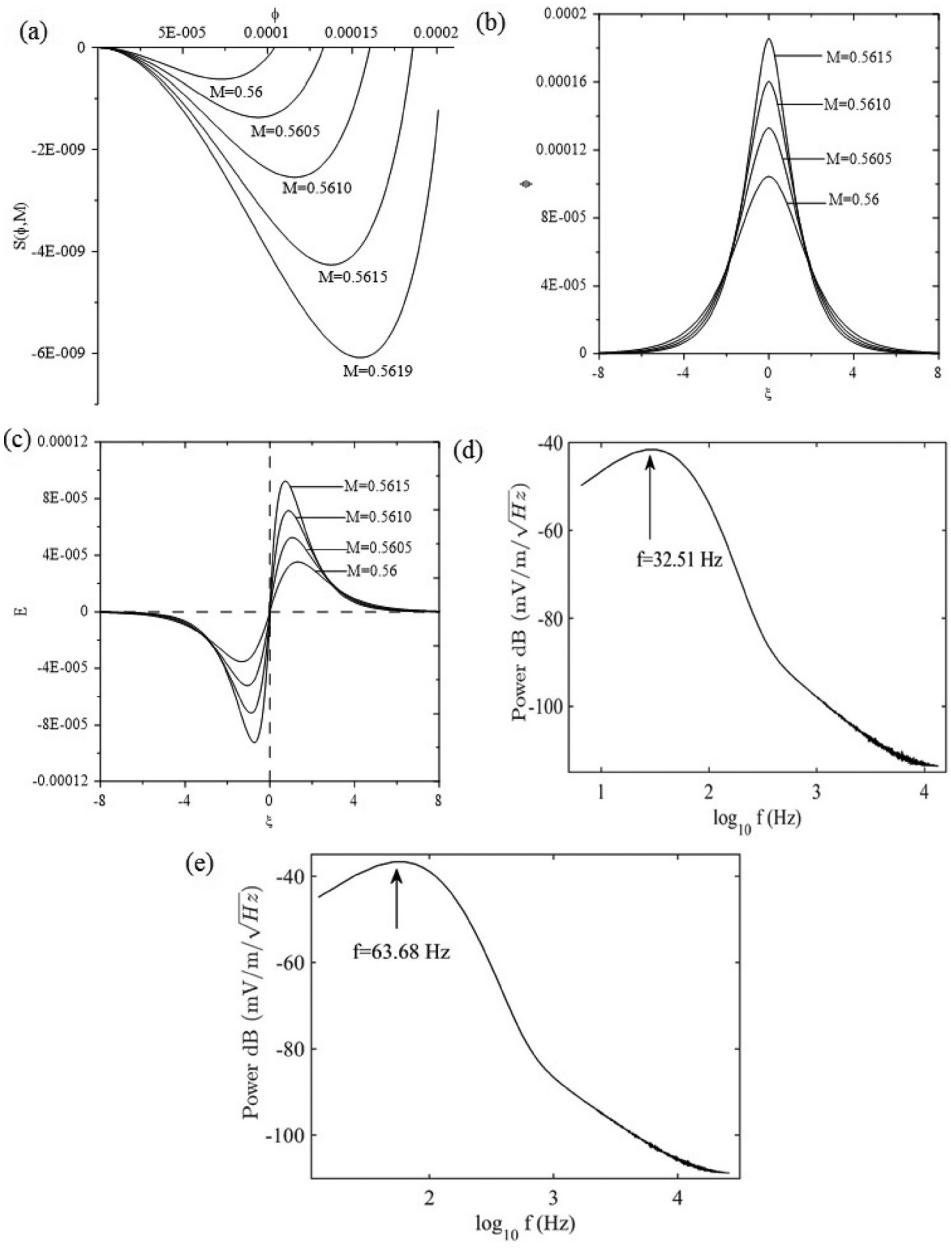

FIG. 9. Slow ion-acoustic mode. Run 1: normalized parameters are $n_{i0} = 0.05$, $n_{p0} = 0.9$, $n_{b0} = 0.01$, $n_{e0} = 0.99$, $\sigma_p = 0.2$, $\sigma_i = 0.4$, $\sigma_b = 0.0025$, $V_{b0} = 17.14$, and $\kappa = 6$. Panel (a) shows the Sagdeev pseudopotential, $S(\phi, M)$ vs the normalized potential ϕ. Panels (b) and (c) show normalized potential, ϕ and normalized electric field, E vs ξ, respectively. The fast Fourier transform (FFT) power spectra of the electric field corresponding to $M = 0.5610$ is shown in panels (d) and (e) for WB1 and WB2/WB3, respectively. The x-axis represents the $\log_{10} f$, where f is the frequency in Hz. The y-axis represents the power of the electric field expressed in units of dB $\left(\mathrm{mV/m/\sqrt{Hz}}\right)$. Reprinted with permission from Rubia *et al.*, J. Geophys. Res. Space Phys. **122**, 9134–9147 (2017). Copyright 2017 John Wiley and Sons.[173]

should be real and is consistent with the results of Rubia *et al.*[171] Panels (b) and (c) show the normalized potential ϕ and electric field amplitude, E, respectively. It is observed that the soliton amplitude increases with the increase in the Mach number, whereas the width decreases. Panels (d) and (e) in Fig. 9 show the fast Fourier transform (FFT) power spectra of the electric field corresponding to the Mach number $M = 0.5610$ for WB1 and WB2/WB3, the three wave bursts, as shown in Fig. 13. The major contribution to power spectra for WB1 comes in the frequency range of ∼(6.5–266.67) Hz, with the peak power at 32.51 Hz. Similarly, for WB2/WB3, the maximum contribution to the power spectra comes from ∼(12.76 to 650.13) Hz frequencies. The peak in the power spectra occurs at 63.68 Hz. It must be pointed out here that in both the cases of WB1 and WB2/WB3, the upper limit on the frequency, f, is taken at the cutoff power of –80 dB.

In Fig. 10, the results for run 1 parameters are presented for both the bursts WB1 and WB2/WB3 for fast ion-acoustic solitons. We show variation of Sagdeev potential versus electrostatic potential in panel (a) for various values of the Mach number. It is noted that the upper limit on the Mach number M_{max} for which soliton solutions are found is provided by the restriction that the lighter ion density n_p should be real and confirms the findings of Rubia *et al.*[171] The normalized potential and the electric field are shown in panels (b) and (c), respectively. The FFT power spectra of the electric field for WB1 and WB2/WB3 are shown in panels (d) and (e), respectively, for the Mach number, $M = 1.275$. For WB1 and WB2/WB3, the frequencies in the range of ∼(14.79–620.87) Hz and ∼(28.97–1940.88) Hz, respectively, contribute maximum to the electric structures. The cutoff power is considered as –30 dB in this case. The peak in the power spectra occurs at a frequency of 29.58 Hz for WB1 and at 57.94 Hz for WB2/WB3 parameters, respectively. Further, both slow and fast ion-acoustic solitons have positive polarity for these parameters.

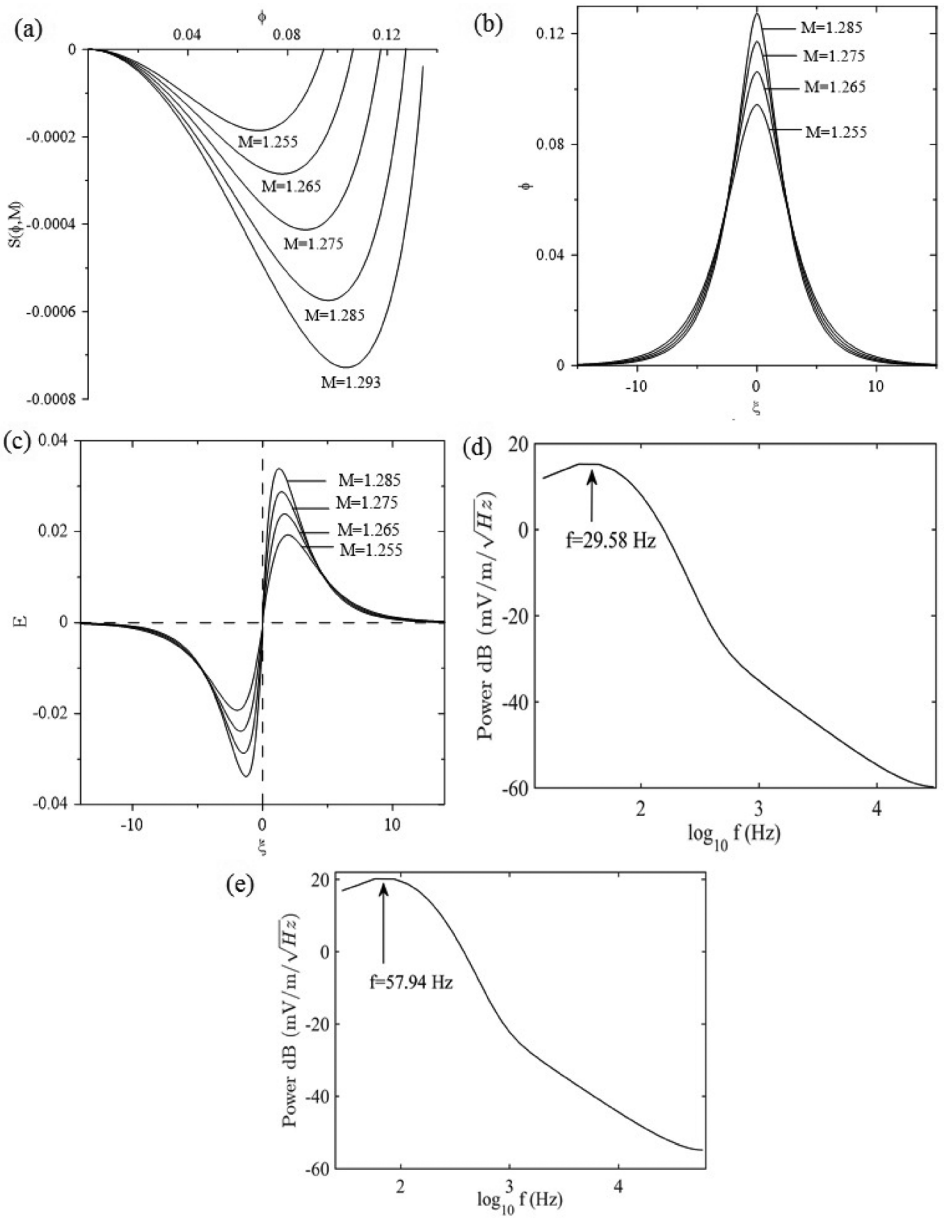

FIG. 10. Fast ion-acoustic mode. Run 1: Panel (a) shows the Sagdeev pseudopotential $S(\phi, M)$ vs the normalized potential ϕ. Panels (b) and (c) show normalized potential ϕ and normalized electric field, E vs ξ, respectively. Panels (d) and (e) show the FFT power spectra of the electric field corresponding to $M = 1.275$ for WB1 and WB2/WB3, respectively. Reprinted with permission from Rubia *et al.*, J. Geophys. Res. Space Phys. **122**, 9134–9147 (2017). Copyright 2017 John Wiley and Sons.[173]

The highest positive root of Eq. (12) corresponds to the electron-acoustic solitons for run 1 parameters presented earlier, and it supports negative potential solitons as seen in Fig. 11. This is in sync with the sign of third derivative of the Sagdeev potential [given by (9)] evaluated at $M = M_0$. In this case, the upper limit on the Mach number, M_{max}, is imposed by the electron beam density, n_b, being real. The behaviours of the Sagdeev potential [panel (a)], electrostatic potential [panel (b)], and electric field [panel (c)] in Fig. 11 are similar to those observed for slow and fast ion-acoustic solitons. The fast Fourier transform power spectra of the electric field corresponding to the Mach number $M = 22.95$ for WB1 and WB2/WB3 are plotted in panels (d) and (e), respectively. The maximum contribution to the electric field structure for WB1 comes from the frequencies ∼(266.07–10641) Hz, whereas for WB2/WB3, it comes from the frequencies in the range of ∼(521.19–35481.33) Hz. The peak power in the power spectra occurs at a frequency of 797.99 Hz for WB1 and 1563.15 Hz for WB2/WB3. Here, the cutoff power is taken as –60 dB and the power spectrum becomes noisy beyond 50 kHz.

IV. APPLICATIONS OF SOLITARY WAVE MODELS TO ESWs IN THE SOLAR WIND AND LUNAR WAKE

Here, we shall discuss the applications of the three- and four-component fluid models developed in Sec. III to the observations of coherent low-frequency waves and weak double layers in the solar wind and the electrostatic turbulence in the lunar wake, respectively.

A. Coherent low-frequency electrostatic waves and weak double layers in the solar wind

1. Observations

The time domain sampler (TDS) on board the Wind spacecraft collects the high-time resolution electric field data in the solar wind at 1 AU.[52,53,181,182] The analysis of TDS data has shown the presence of three kinds of electrostatic waves, namely, coherent wave packets of Langmuir waves with frequencies $f \sim f_{pe}$ (electron plasma frequency), coherent wave packets in the ion-acoustic frequency range with f_{pi} (ion plasma frequency) $< f \sim f_{pe}$, and isolated non-sinusoidal

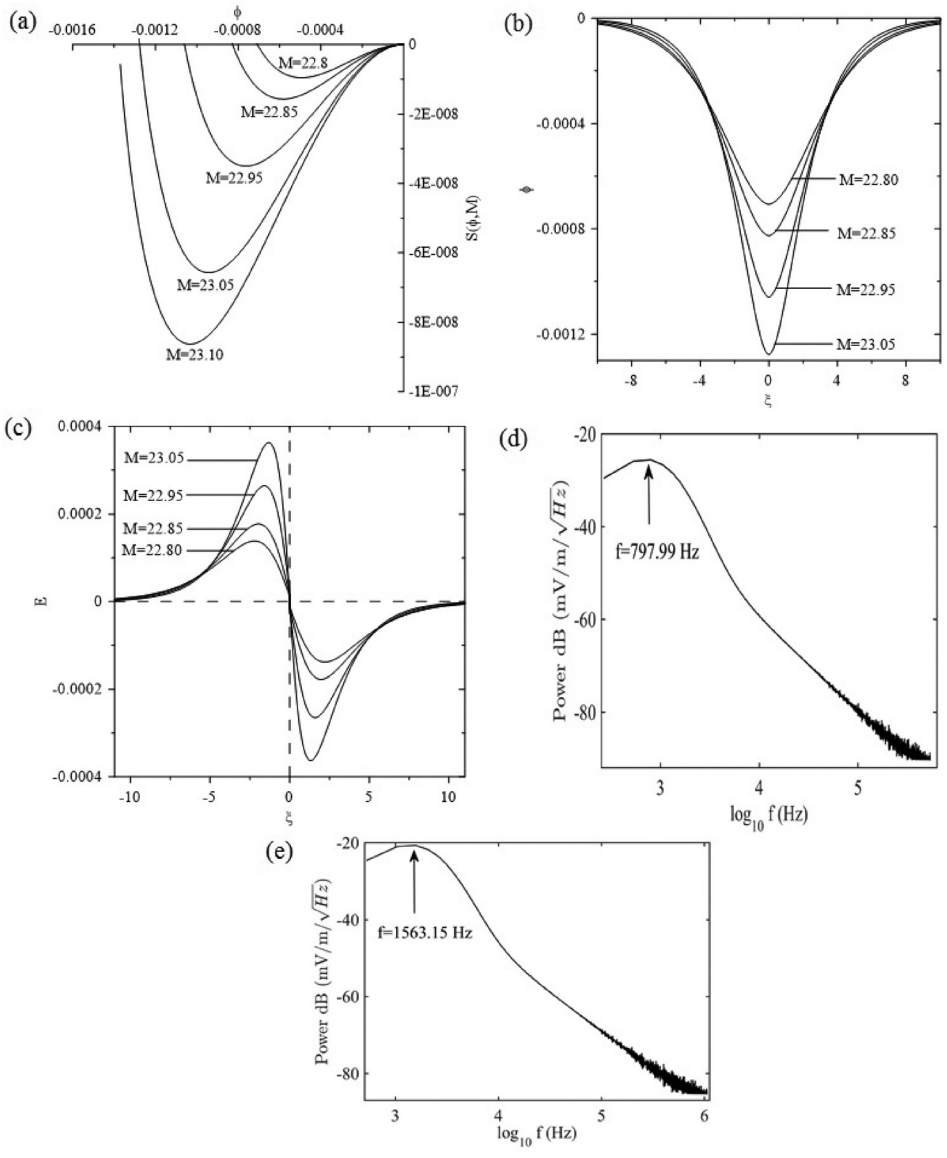

FIG. 11. Electron-acoustic mode. Run 1: Panel (a) shows the plot of Sagdeev pseudopotential $S(\phi, M)$ vs the normalized potential ϕ. Panels (b) and (c) show normalized potential ϕ and normalized electric field E vs ξ, respectively. Panels (d) and (e) show the FFT power spectra of the electric field corresponding to $M = 22.95$ for WB1 and WB2/WB3, respectively. Reprinted with permission from Rubia *et al.*, J. Geophys. Res. Space Phys. **122**, 9134–9147 (2017). Copyright 2017 John Wiley and Sons.[173]

solitary structures lasting for less than 1 ms.[52,181,182] The typical waveforms of these three electrostatic waves are illustrated in Fig. 12 which displays six typical TDS events observed by wind at 1 AU on different days.[52] In Fig. 12, panel (a) shows the typical Langmuir wave packets, panels (b) and (c) illustrate the typical low-frequency quasi-sinusoidal wave packets of coherent ion acoustic waves, and panels (d)–(f) display the non-sinusoidal wave packets and isolated electrostatic solitary structures (generally having a tripolar pulse shape). Mangeney *et al.*[52] analysed the coherent ion-acoustic wave packets and isolated electrostatic structures. They found that the electric fields of the coherent ion-acoustic waves are nearly aligned parallel to the magnetic field, and their amplitudes are $\sim$(0.0054–0.54) mV m^{-1}. They also found that isolated electrostatic solitary structures carry a net potential drop of $\approx$1 mV (directed towards the Earth); these were interpreted in terms of weak double layers (WDLs). About 30% of the coherent low-frequency electrostatic waves in the TDS data are found to be WDLs, with a typical spatial size of $\sim$25 λ_D (Debye length).[52,181,182]

Malaspina *et al.*[53] have analysed the Wind/TDS data and reported a strong spatial association between bipolar electrostatic solitary waves (ESWs) and magnetic current sheets (CSs) in the solar wind at 1 AU. The ESW peak-to-peak amplitudes were found to range from 0.1 mV m^{-1} to 8 mV m^{-1} with an average of 0.5 mV m^{-1}. They interpret the faster moving ESWs as the electron holes.

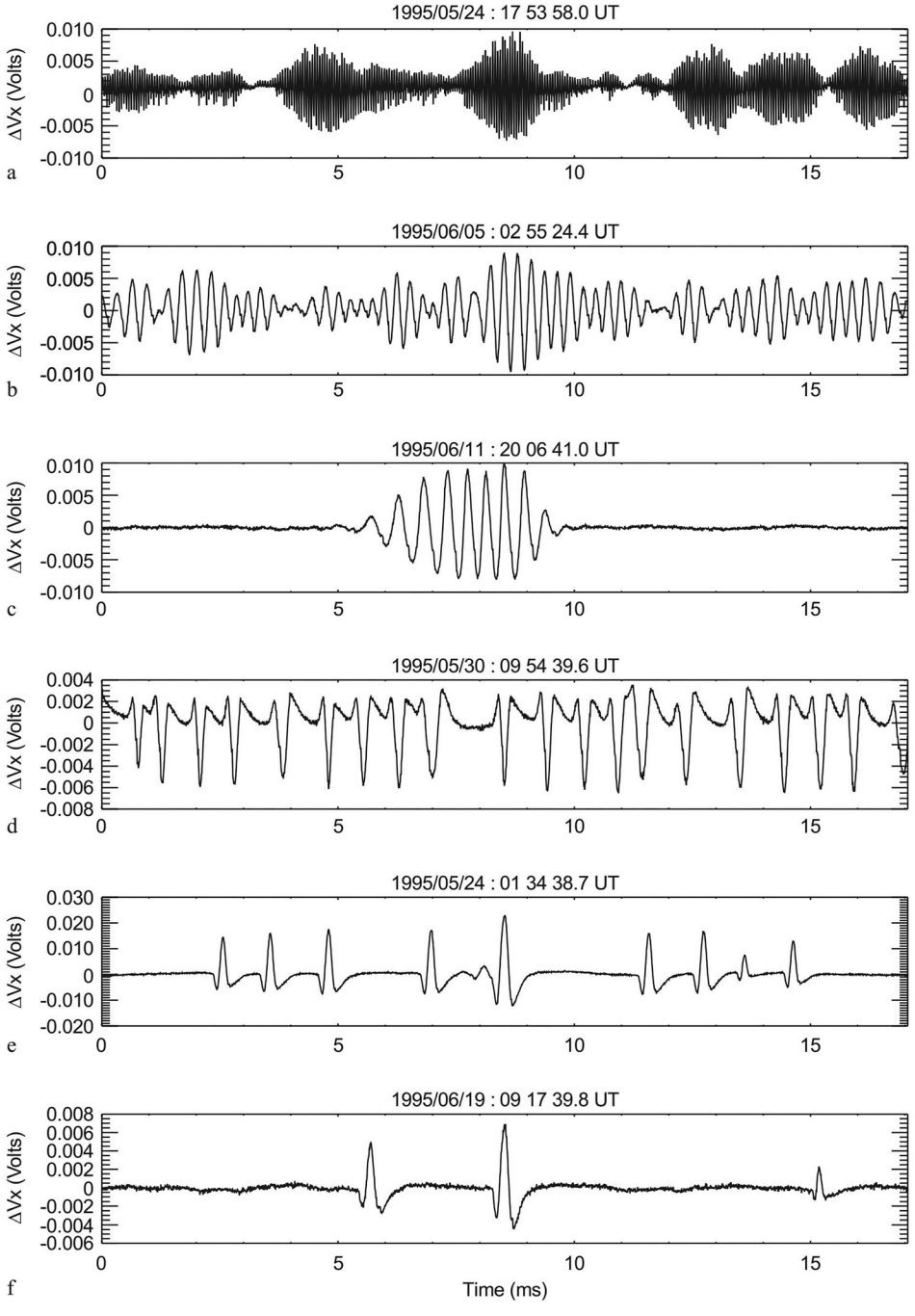

FIG. 12. Six typical wave forms observed by the TDS on board Wind spacecraft in the solar wind at 1 AU. The electric potential ΔV_x in volts is along the y-axis and time is shown along the x-axis. Panel (a) shows the Langmuir waves; panels (b) and (c) show low-frequency quasi-sinusoidal wave packets of coherent ion acoustic waves; and panels (d), (e), and (f) display non-sinusoidal wave packets and isolated electrostatic solitary structures. Reprinted with permission from Mangeney *et al.*, Ann. Geophys. **17**, 307–320 (1999). Copyright 1999 European Geosciences Union.[52]

2. Predictions of three component solar wind theoretical model

From Figs. 5 and 7, it is seen that the maximum amplitudes of slow ion-acoustic solitons (double layers) vary over a wide range of $\phi_{max} = 5 \times 10^{-6}$ to 0.0015 (0.001 to 0.005) for positive potential structures, and $\phi_{max} = -10^{-6}$ to –0.0035 (-2.0×10^{-4} to –0.0055) for the negative potential structures with Mach numbers in the range of $M = 0.9$ to 2.54. The widths of slow ion-acoustic solitons/DLs vary over a range of $W \sim$ (7–34). Figure 6 shows that the maximum amplitudes of fast ion-acoustic solitons vary over a range of $\phi_{max} = 2 \times 10^{-6}$ to 0.012 with Mach numbers in the range $M = 1.01$ to 2.65. Considering a typical ion-acoustic speed $C_a = 31\,\text{km s}^{-1}$ in the solar wind at 1 AU, the slow and fast ion-acoustic solitons/DLs will have speeds varying from 28 to 78 km s^{-1} and 31 to 82 km s^{-1}, respectively. Therefore, these solitary structures will be convected with the solar wind flow.

3. Comparison of theoretical predictions with the observations

We shall now discuss the relevance of above theoretical results to the observation of non-sinusoidal isolated spikes and coherent electrostatic waves consisting of quasi-sinusoidal structures in the solar wind at 1 AU. As stated earlier, isolated non-sinusoidal spiky structures have been interpreted as weak double layers (WDLs). The typical values of the potential drops across the WDLs[52,181,182] in the solar wind at 1 AU are found to be $e\phi/T_e \sim 10^{-4}$–10^{-3}. Whereas the negative DLs found here have $\phi_{max} = -2.0 \times 10^{-4}$ to –0.0055 and cover the potential drop range observed in the solar wind. However, the positive potential DLs have $\phi_{max} = 0.001$ to 0.005, which is above the typical values of the observed potential drops. However, this is just a minor problem as changing some parameters, e.g., taking higher values of T_p and higher T_i/T_p ratios, and varying the values of the κ index and α-proton relative streaming velocity, U_0, one obtains positive DLs with lower magnitudes. Actually, the major problem seems to be the disagreement between the shapes of the observed weak double layer and the DLs found in the model. The observed WDL's profile shows initially a gradual decrease, then a sharp dip to negative values followed by a recovery to positive values, which slowly decrease to zero.[52] The DLs found here start from positive (negative) values and decrease smoothly to values approaching zero. There is no dip in the potential. It appears as if the observed WDL profiles are made up from the fusion of a positive DL and a negative potential soliton! Further, the widths of the four DLs analysed in Fig. 5 are $W = 20.0$, 13.0, 27.5, and 12 (in units of electron Debye length λ_{De}). Thus, the predicted widths of slow ion-acoustic DLs show an excellent agreement with the observed WDLs widths spanning a range of 5 to 60 λ_{De} with a peak around 25 λ_{De}.[52]

Furthermore, the slow ion-acoustic mode DLs predicted by our model are moving with speeds of ~(28–78) km s^{-1}, which are much smaller than the flow speeds of the slow solar wind streams (~350 km s^{-1}). There are no measurements of the flow speed of WDLs observed in the solar wind at 1 AU. The observed WDLs are found to be propagating parallel to the local magnetic field, but their relative speed compared to solar wind is taken as negligible.[52,181] The double layers studied here may be relevant in heating the solar wind protons[177] and in maintaining the interplanetary electric field parallel to the spiral interplanetary magnetic field as suggested by Mangeney *et al.*,[52] Lacombe *et al.*,[181] and Salem *et al.*[182]

The coherent low-frequency electrostatic wave activity observed in the solar wind at 1 AU by the *Wind* spacecraft can be directly explained by the presence of both slow and fast ion-acoustic solitons, which are coherent structures. The fast Fourier transform (FFT) of the ion-acoustic solitons can generate a broadband spectrum with a main peak near the inverse of the duration time, τ, of soliton pulse felt by the measuring instruments on the spacecraft. The duration time τ can be easily calculated (in unnormalized units, i.e., in seconds) as[170]

$$\tau = \frac{W}{f_{pp}\left(\frac{V_{sw}}{C_a} - M\right)}, \tag{13}$$

where f_{pp} is the proton plasma frequency in Hz. As an illustration, let us calculate the soliton pulse duration for the slow ion-acoustic solitons/DLs shown in Fig. 5. Considering a solar wind speed $V_{sw} = 700\,\text{km s}^{-1}$, electron temperature of $T_e = 10\,\text{eV}$, and electron density of $N_e = 7.75\,\text{cm}^{-3}$ corresponding to the observed electron plasma frequency $f_{pe} = 25\,\text{kHz}$,[52] we get $C_a = 31\,\text{km s}^{-1}$, $f_{pp} = 585\,\text{Hz}$, $\lambda_{De} = 840\,\text{cm}$, and $V_{sw}/C_a = 22.6$. Then, the soliton pulse durations for the slow ion-acoustic solitons/DLs shown in Fig. 5 will be for panel (a): $\tau = 2.7\,\text{ms}$, 2.3 ms, 2.5 ms, and 1.6 ms; panel (b): $\tau = 0.6\,\text{ms}$, 0.7 ms, 0.9 ms, and 1.1 ms; panel (c): $\tau = 2.6\,\text{ms}$, 2.6 ms, 2.7 ms, and 2.2 ms; and panel d: $\tau = 1.5\,\text{ms}$, 1.4 ms, 1.5 ms, and 1.0 ms, respectively, to curves 1, 2, 3, and 4, in each panel of Fig. 5. Consequently, the broadband low-frequency electrostatic waves produced by the coherent slow ion-acoustic solitons/DLs would have first peaks between 0.35 kHz and 1.6 kHz. The electric fields of these waves as calculated from Fig. 8 would lie in the range of $E = 0.01$–0.7 mV m^{-1} which are in excellent agreement with the observed electric fields ~(0.0054–0.54) mV m^{-1} associated with the low-frequency waves observed in the solar wind at 1 AU.[52] Incidentally, these estimates of the electric field amplitude match with the average E amplitudes of the ESWs as observed by Malaspina *et al.*[53]

B. ESWs and electrostatic waves in the lunar wake

1. Observations

When the solar wind interacts with the Moon, the solar wind plasma is absorbed by the lunar surface carving out a depleted wake region in the "nightside" of the Moon, referred as the lunar wake. The density gradient between the solar wind and the lunar wake drives the solar wind plasmas to refill the lunar wake along the magnetic field lines.

Electrons being lighter rush into the wake region ahead of the ions resulting in a negatively charged wake region. The potential gradient in the wake results in an ambipolar

electric field that accelerates the ions into the wake.[180,183,184] Electrostatic wave turbulence and ESWs have been observed in the lunar wake. From the analysis of the waveform capture data collected by the KAGUYA spacecraft in the lunar wake on April 2, 2008, Hashimoto *et al.*[54] reported the presence of ESWs in the electric field component parallel to the magnetic field. These ESWs have peak to peak amplitudes of ∼a few mV m^{-1}.

Earlier, a simple 1D electrostatic particle-in-cell (PIC) simulation model has predicted the excitation of kinetic instabilities in the lunar wake.[185] Also, electron phase space holes travelling away from the wake along the interplanetary magnetic field lines have been seen in 1-D and 2-D PIC simulations of the wake.[186,187]

Figure 13 displays an overview of the observations of the first lunar wake flyby by the Acceleration, Reconnection, Turbulence, and Electrodynamics of the Moon's Interaction with the Sun (ARTEMIS) mission on February 13, 2010.[180] The ARTEMIS mission is a new two-probe lunar mission derived from THEMIS (Time History of Events and Macroscale Interactions during Substorms) mission. The two vertical black dashed lines in Fig. 13 correspond to the interval in which the ARTEMIS P1 crossed the lunar shadow. Panel (a) indicates the exponential decrease in the density towards the center of the wake. Panel (b) shows the ion velocity in Selenocentric Solar Ecliptic (SSE) coordinates. The flow velocity is found to be relatively stable during the flyby. The variation in electron temperature T_e is found to be nearly isotropic outside the wake [panel (c)], while both the field-aligned temperature and perpendicular temperature increase inside the wake, with the former increasing more. Panels (d) and (e) show the observed magnetic field (in SSE coordinates) and the differential energy flux of the parallel electrons, respectively. Panel (f) depicts the electric field power spectrum. The frequency of the electrostatic waves was found to be ∼(0.1–0.4) f_{pe}. However, in the middle of the flyby, the power occasionally reduces to 0.01 f_{pe}, where f_{pe} is the electron plasma frequency. These waves were interpreted as electrostatic waves as no corresponding magnetic field signals were observed. The black vertical lines across panels (e) and (f) specify the times of the three high time resolution wave bursts. The three wave bursts are labelled as

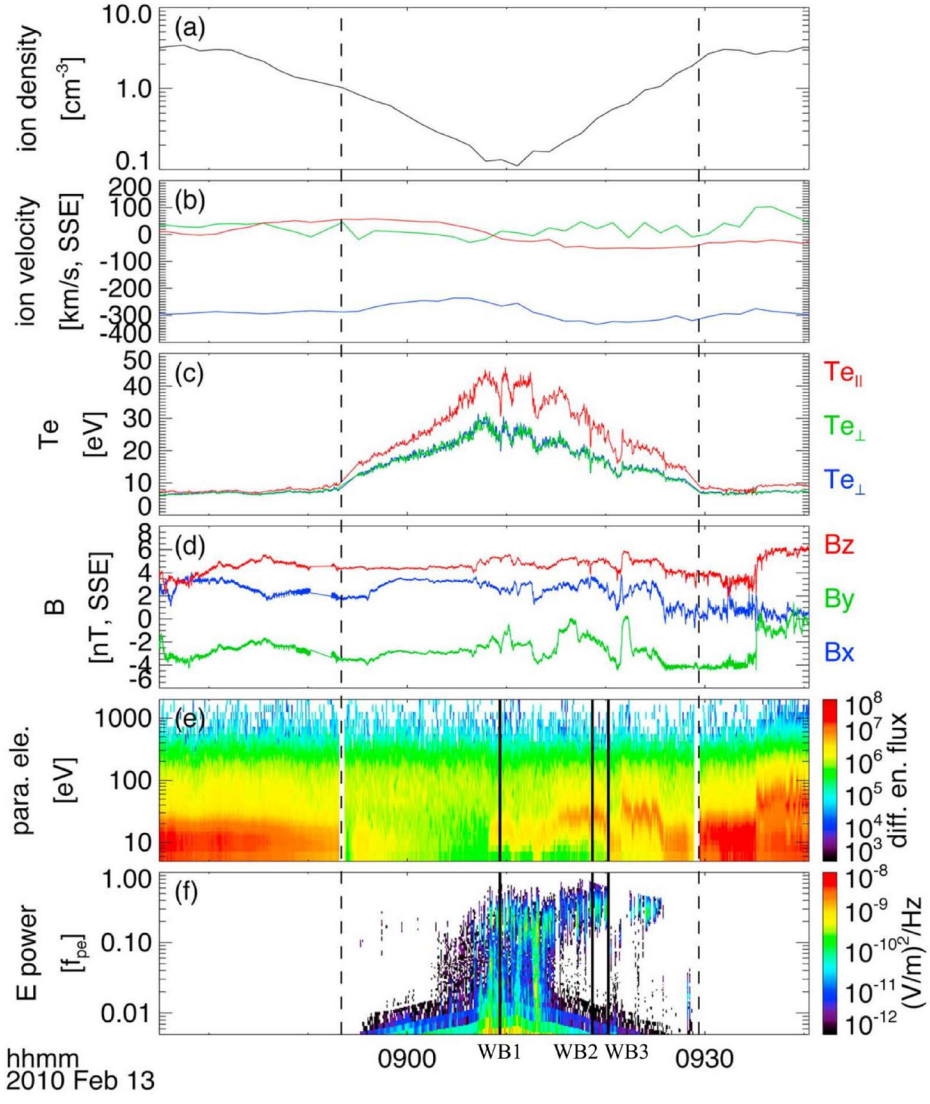

FIG. 13. An overview of the observations of the first lunar wake flyby of the ARTEMIS mission. The two vertical dashed lines correspond to the duration in which the flyby crossed the lunar shadow. (a) Ion density. (b) Ion velocity in Selenocentric Solar Ecliptic (SSE) coordinates. (c) Electron temperature. Here, the red line corresponds to the field-aligned temperature ($T_{e\|}$) and the green and blue lines correspond to the perpendicular temperatures ($T_{e\perp}$). The green line fully overlaps the blue line as there is no special preference in perpendicular temperatures. (d) Magnetic field in SSE coordinates. (e) Differential energy flux of parallel electrons. (f) Electric field power spectrum from the onboard digital field board (DFB). Here, frequency is normalized by the local electron plasma frequency (f_{pe}). The three vertical bars in panels (e) and (f) indicate the times of three wave bursts. These wave bursts are designated as WB1, WB2, and WB3 according to their temporal order of occurrence Reprinted with permission from Tao *et al.*, J. Geophys. Res. **117**, A03106 (2012). Copyright 2012 John Wiley and Sons.[180]

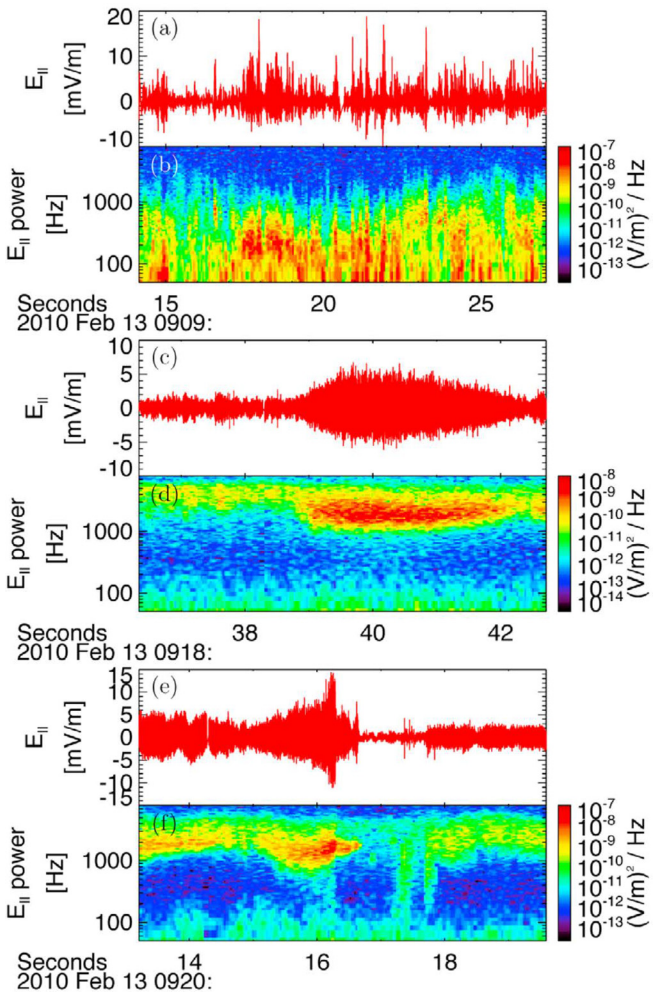

FIG. 14. Parallel electric field waveforms and spectrograms of wave bursts, WB1 [(a) and (b)], WB2 [(c) and (d)], and WB3 [(e) and (f)]. Reprinted with permission from Tao *et al.*, J. Geophys. Res. **117**, A03106 (2012). Copyright 2012 John Wiley and Sons.[180]

WB1, WB2, and WB3 in a temporal order of their occurrence as shown in Fig. 13.

Figure 14 shows the waveforms in the frequency range from ~10 Hz to ~6 kHz and spectrograms of parallel electric fields ($E_{\|}$) from wave bursts WB1 [panels (a) and (b)], WB2 [panels (c) and (d)], and WB3 [panels (e) and (f)] as given in Fig. 3 of Ref. 180. It is seen that the electric field, **E**, of these electrostatic waves is parallel to the ambient magnetic field, $\mathbf{B}_0$ ($\mathbf{E} \parallel \mathbf{B}_0$), and further these waves propagated along $\mathbf{B}_0$ ($\mathbf{k} \parallel \mathbf{B}_0$), where **k** is the propagation vector. The electric field amplitude of these electrostatic waves seems to be in the range of ~(5–15) mV m^{-1}.

From the cross-correlation analysis, Tao *et al.*[180] estimated the phase velocities of the waves to be of the order of 1000 km s^{-1}. On the basis of cross-spectrum analysis, they estimated the wavelengths to vary from a few hundred meters to a couple of thousand meters. The local values of Debye length, λ_D, was found to be roughly 108, 53, and 46 m for WB1, WB2, and WB3, respectively. Tao *et al.*[180] carried out 1-D Vlasov simulation of a four-component plasma, comprising of protons, ions, both an electron beam and background electrons following kappa-distribution, to explain the physical properties of the observed electrostatic waves. On the basis of the simulation, they concluded that the observed waves in the frequency range ~(0.1–0.4) f_{pe} were most likely the electron beam mode. However, they were unable to explain the observed low frequency waves with frequencies ~0.01 f_{pe}. Further, though they did not observe well defined ESWs, the probability of the occurrence of the ESWs in the lunar wake was not completely ruled out.

2. Predictions of four component lunar wake theoretical model

The physical properties of the ESWs in terms of unnormalized quantities, such as their polarity, soliton velocities, V (km s^{-1}), electric field, E (mV m^{-1}), soliton width, W (m), and peak frequency, f_{peak} (Hz) corresponding to the maximum power in the frequency spectrum, for both run 1 and run 2, are listed in Tables I and II. For numerical estimation of the physical properties of the electrostatic solitary waves (given in Tables I and II), we have used the observed parameters for the burst WB1: temperature of electron, $T_e = 28$ eV, and the total number density of electrons, $N_0 = 0.13$ cm^{-3}, and for the burst WB2/WB3: $T_e = 22.64$ eV and $N_0 = 0.5$ cm^{-3}, as given in Ref. 180. This gives for the burst WB1 (WB2/WB3), the ion-acoustic speed, $C_a = 52$ km s^{-1} (46 km s^{-1}), the hot electron Debye length, $\lambda_{de} = 109$ m (50 m), and the proton plasma frequency, $f_{pp} = 474.69$ Hz (930.95 Hz), respectively.

TABLE I. Properties of electrostatic solitary waves for run 1 parameters corresponding to wave bursts WB1 and WB2/WB3. For WB1: temperature of κ - electron, $T_e = 28$ eV, total equilibrium electron number density, $N_0 = 0.13$ cm^{-3}, electron plasma frequency, $f_{pe} = 3237.78$ Hz, ion-acoustic speed, $C_a = 52$ km s^{-1}, the effective hot electron Debye length, $\lambda_{de} = 109$ m and for WB2/WB3, $T_e = 22.64$ eV, $N_0 = 0.5$ cm^{-3}, $f_{pe} = 6349.82$ Hz, $C_a = 46$ km s^{-1}, and $\lambda_{de} = 50$ m. Here and in Table II, V is soliton velocity, E is electric field, W is soliton width, and frequency f_{peak} corresponds to peak power in the spectrum. Reprinted with permission from Rubia *et al.*, J. Geophys. Res. Space Phys. **122**, 9134–9147 (2017). Copyright 2017 John Wiley and Sons.[173]

		WB1				WB2/WB3			
Mode	Polarity	V (km s^{-1})	E (mV m^{-1})	W (m)	f_{peak} (Hz)	V (km s^{-1})	E (mV m^{-1})	W (m)	f_{peak} (Hz)
Slow ion-acoustic	+ve	28.91-29.08	0.0003-0.026	1330.76-261.79	6.47-34.2	26-26.15	0.0005-0.046	610.16-120.03	12.7-66.99
Fast ion-acoustic	+ve	61.86-113.89	0.0082-9.52	7439.19-479.95	3.46-41.11	55.64-60.11	0.0145-16.79	3410.92-220.06	5.09-80.92
Electron-acoustic	–ve	1169.48-1195.37	0.0043-0.104	1243.5-436.316	261.81-803.530	1051.79-1075.07	0.0076-0.1832	570.15-200.05	512.86-1573.98

TABLE II. Properties of electrostatic solitary waves for run 2 parameters corresponding to wave bursts WB1 and WB2/WB3. The parameters corresponding to WB1 and WB2/WB3 are same as listed in Table I. Reprinted with permission from Rubia *et al.*, J. Geophys. Res. Space Phys. **122**, 9134–9147 (2017). Copyright 2017 John Wiley and Sons.[173]

		WB1				WB2/WB3			
Mode	Polarity	V (km s^{-1})	E (mV m^{-1})	W (m)	f_{peak} (f_{pe})	V (km s^{-1})	E (mV m^{-1})	W (m)	f_{peak} (f_{pe})
Slow ion-acoustic	+ve	28.92-29.09	0.0004-0.027	1221.68-239.97	6.47-34.2	26.01-26.16	0.0008-0.047	560.15-110.03	12.7-66.99
Fast ion-acoustic	+ve	63.00-67.34	0.038-9.7	6501.11-479.95	2.64-41.5	56.66-60.56	0.066-17.106	2980.8-220.06	6.92-77.62
Fast ion-acoustic	–ve	63.00-63.78	0.019-0.58	8028.21-1112.605	2.64-17.86	56.66-57.36	0.033-1.028	3680.99-510.14	3.46-34.99
Electron-acoustic	–ve	1348.09-1368.79	0.004-0.07	1199.87-436.32	591.56-1803.02	1212.42-1231.05	0.007-0.12	550.15-200.05	591.56-1803.02

In Tables I and II, the soliton width, W, is defined as the full width at half maximum, and the lower value of the peak frequency, f_{peak}, corresponds to the peak power in the spectrum of lower velocity soliton.

Combining the results of run 1 and run 2 as shown in Tables I and II, it is clear that for electron-acoustic solitons, the soliton velocities vary from ∼1050 to 1370 km s^{-1}, the soliton widths vary from ∼200 to 1243 m, maximum electric fields vary ∼(0.004–0.18) mV m^{-1}, and the peak frequencies fall in the range of ∼(261–1803) Hz corresponding to ∼(0.08–0.56) f_{pe}. Here, the higher value of the soliton width corresponds to the lower soliton velocity. For slow ion-acoustic solitons, the soliton velocities are in the range of ∼(26–29) km s^{-1}, the soliton widths are ∼(110–1330) m, maximum electric fields are ∼(0.0003–0.047) mV m^{-1}, and the peak frequencies are in the range of ∼(6–67) Hz which corresponds to $f \sim$ (0.002–0.01) f_{pe}. It is interesting to note that for the case of run 2 parameters, both positive as well as negative polarity fast ion-acoustic solitons coexist. For positive potential fast ion-acoustic solitons, the soliton velocities, widths, maximum electric fields, and peak frequencies are in the range of 55–114 km s^{-1}, 220–7439 m, and 0.008–17 mV m^{-1}, and peak frequencies are in the range of ∼(3–80) Hz corresponding to $f \sim$ (0.0008–0.01) f_{pe}, respectively. On the other hand, for negative potential fast ion-acoustic solitons, the maximum electric field amplitude and peak frequencies are less than the positive potential ion-acoustic waves; however, the widths are a bit larger. Usually, positive polarity solitons are supported by fast ion-acoustic modes,[96,170,171] however, for the first time, the coexistence of both positive and negative polarity fast ion-acoustic solitons is observed in the presence of κ– electrons.

3. Comparison of theoretical predictions with the observations

We shall now discuss how the theoretical predictions of the four component lunar wake model compare with the electrostatic wave observations during ARTEMIS first flyby of the lunar wake on February 13, 2010.[180] For the plasma parameters in the lunar wake corresponding to the wave bursts WB1 and WB2/WB3, our model predicts the simultaneous existence of slow and fast ion-acoustic and electron-acoustic solitons. The FFT of these solitons will produce power spectra which have peaks between ∼(3 and 1800) Hz (see Tables I and II, and discussion above). Then, the maximum wave power would correspond to frequencies ∼(0.001–0.56) f_{pe}. This is in excellent agreement with the observed low-frequency electrostatic waves with the frequency ∼0.01 f_{pe} at WB1 and the high-frequency waves with frequencies of ∼(0.1–0.4) f_{pe} at WB1 and WB2/WB3 in the lunar wake.[180] Furthermore, considering properties of the slow and fast ion-acoustic and electron-acoustic solitons together, we note that the soliton widths, electric field amplitudes, and velocities are in the range of ∼(100–8000) m, ∼(0.0003–17) mV m^{-1}, and ∼(30–1300) km s^{-1}, respectively. These values appear to be in good agreement with the wavelengths (a few hundred meters to a couple of thousand meters), electric field amplitudes (5–15 mV m^{-1}), and phase velocities (∼1000 km s^{-1}) of the electrostatic waves observed in the lunar wake.[180]

V. SUMMARY AND DISCUSSION

We first give an overview of the main characteristics of the broadband electrostatic noise (BEN)[1–6,9,10,12,13,16] and the electrostatic solitary waves (ESWs)[20–22] observed in various regions of the Earth's magnetosphere. It is interesting to note that both BEN and ESWs were observed in the same regions, but no connection between them was made for more than a decade by the space community. The reason being that while BEN emissions were studied employing frequency spectrum, the ESWs were being studied in time domain. From the analysis of the high time resolution waveform observations by the plasma wave instrument on board the Geotail spacecraft,[23] Matsumoto and his colleagues were the first to establish a connection between the two. They showed that BEN consists of a series of bipolar pulses and that the broadness of the BEN frequency spectra arises from FFT of these solitary waveforms or ESWs. It is interesting to point out that ESWs have also been observed in Europa's wake during Galileo flyby of Jupiter[188] and at Saturn bow-shock crossings during June 27–29, 2004, by Cassini.[189]

Next, the highlights of the two most popular models of ESWs, namely, BGK Modes/Phase Space Holes and Solitons/Solitary Waves, are discussed emphasizing the pros

and cons of these models in explaining the ESWs observations in space. It is followed by the development of fluid models for ion-and electron-acoustic solitons and double layers in multi-component plasmas containing suprathermal electrons having κ-distribution function. Two special cases, namely, a three component fluid model for the solar wind and a four component model for the lunar wake plasma, are discussed. In the former model, only slow and fast ion-acoustic solitons/double layer exist, whereas in the latter model, slow and fast ion-acoustic and electron-acoustic solitons occur. Next, observations of coherent low-frequency electrostatic waves and weak double layers in the solar wind at 1 AU and the electrostatic turbulence in the lunar wake are summarized. Then, the predictions of these models are compared with the observations. The theoretical predictions of the fluid models can explain the main characteristics of the electrostatic waves observed in the solar wind and lunar wakes in terms of slow and fast ion-acoustic and electron acoustic solitons. At the same time, these models could provide a plausible explanation for the ESWs observed in the solar wind and the lunar wake.[53,54] Furthermore, the fluid models discussed here are quite general and can be applied to many space and astrophysical situations where two types of ions (or even ion and positron combination), electron beams, and suprathermal electrons described by κ-distribution function are present.

We must emphasize that the solitary wave models discussed here are based on the Sagdeev pseudopotential method. This technique deals with the time stationary solutions of the fluid equations when the system has reached the equilibrium state, just like the BGK modes which are the time stationary solutions of the Vlasov-Poisson equations. This means that if there were any instabilities in the system (due to any free energy source), they have been already saturated and stabilized. Therefore, the Sagdeev potential technique does not tell us about the free energy sources. But, it gives soliton solutions, which are the nonlinear eigenmodes of the system, under certain conditions. Furthermore, the effects of trapped particle populations are neglected in fluid models. The fluid models are justified for scale lengths greater than the Debye length. Therefore, these models cannot accurately describe the properties of ESWs having widths of the order of Debye length or less.

To the best of our knowledge, the phase space electron (ion) holes have not been observed in any space observation of ESWs, though they have been predicted theoretically as well as seen in simulations.[55,59–64,69,70,101] The reason for not observing the phase space holes may simply be due to the limitation on the resolution of the instruments measuring particle velocity distribution function. As the phase space holes manifest a strongly nonlinear process involving electron trapping, this could lead to electron density depletions in the real space. In a multi-electron component plasma, the electron species trapped in the phase space hole will show depletion in density whereas the un-trapped electron species may develop a hump in density in the real space. In a multi-component plasma, the ion and electron-acoustic soltions can also produce ion or electron density humps/depletions in the real space. Therefore, it is difficult to distinguish between the phase space hole models or soliton models being responsible for the observed ESWs in space plasmas.

We would like to emphasize that the prediction of the nonlinear fluid soliton models based on Sagdeev pseudopotential technique has been confirmed by the one-dimensional fluid simulation of the ion-acoustic solitons propagating parallel to the magnetic field in electron-ion plasmas with or without the superthermal electron component.[190–192] Kakad *et al*. have performed both fluid and particle-in-cell (PIC) one-dimensional simulations of the ion-acoustic solitary waves in a plasma. They find that the results from the fluid and PIC simulations are in close agreement when the initial density perturbation to initiate the simulations is small. However, when the initial density perturbation is large, there is a discrepancy between the two models; the fluid simulations tend to overestimate the magnitude, width, and speed of the ion-acoustic solitons as compared to PIC simulations.[193,194] This discrepancy could be due to absence of trapping in fluid simulations. Recent 1-D PIC simulations of the head-on collisions of multiple counter-streaming coherent phase space structures, associated with ion-acoustic solitary waves in plasmas, show that they emerge out from each other retaining their characteristics, thus following a soliton type behaviour. Interestingly, while the electrons trapped inside the solitary wave potential are accelerated, the ions are decelerated during the collisions of phase space structures.[195]

The other point we would like to stress upon is that the arbitrary amplitude (fully nonlinear) soliton models discussed here are one dimensional (1D) and valid for the waves propagating parallel to the ambient magnetic field. For the case of obliquely propagating waves, mostly the weakly nonlinear soliton models exist. But here also the coordinate transformation done to solve the evolution equation renders them effectively dependent on one coordinate, i.e., 1D.[113,168] A little work has been done on the truly two dimensional solitons or *dromions* which are the solution of the so-called Davey-Stewartson-I equation (DS-I),[196] which is a two-dimensional generalization of the nonlinear Schrödinger equation (NLSE). The DS-I equations admit dromion solutions which are generalizations of soliton solutions to two dimensions and exhibit exponential spatial decay in both directions. A parametric characterization of the regions of existence of electron-acoustic dromion solutions in the polar cap boundary layer region has been done by Ghosh *et al*.[197,198] It would be worthwhile to study dromions in other space plasma situations, e.g., auroral field lines, plasma sheet boundary layer, magnetosheath, bow-shock, etc.

Another area worth pursuing would be to investigate the stability of ion- and electron-acoustic solitons to 2D and 3D perturbations. One-dimensional ion-acoustic solitons in a low-β plasma, described by a K-dV equation, are found to be unstable with respect to perturbations perpendicular to their motion.[199] On the other hand, two-dimensional ion-acoustic solitons described by the Kadomtsev-Petviashvili (KP) equation[200] are shown to be stable against 2D perturbation, but unstable for 3D perturbation.[201] However, in a low-β plasma, stable three-dimensional ion-acoustic soliton can exist under

certain conditions.[202] Stability analysis, based on a nonlinear Schrödinger equation, reveals that large amplitude electron-acoustic waves may become modulationally unstable depending on the angle between the modulation and propagation directions. Different types of localized electron-acoustic excitations in the form of bright and dark/grey envelope solitons can exist.[203–205] There are a number of articles dealing with the stability of solitons in space plasmas, fluids, dusty plasmas, electron-positron-ion (e-p-i) plasmas, and even quantum plasmas.[206–218] These references will be helpful to the readers interested in problems of multi-dimensional solitons and their stability against transverse perturbations.

VI. FINAL COMMENTS

Mälkki *et al.*[219] compared the Viking observations of solitary waves and double layers with the ion-acoustic soliton theories[103,220,221] and numerical simulations.[105,222] They concluded that numerical simulations, where ion phase space holes are formed due to current driven instability, are more consistent with the Viking observations rather than the predictions from the ion-acoustic soliton theories. According to them, the main drawback of the soliton theories was that the predicted speeds of the solitary structures were larger than the speeds of the solitary structures observed by the Viking, even when the oxygen ion beam was present.[223] Crumley *et al.*[224] performed PIC simulations of solitary waves using a 2 spatial and 3 velocity dimension electrostatic codes with one electron and two ions (hydrogen and oxygen) species. High resolution data from Polar[37,225] and FAST[226,227] were used as input parameter for these simulations. They find that initially the ion two-stream instabilities excite ion acoustic waves, which grow in amplitudes and first trap H^+ and later on O^+ to form ion phase space holes, which eventually nonlinearly transform into ion-acoustic solitary waves. The speeds of ion-acoustic solitons are greater than the O^+ beam speed but less than the H^+ beam speed. The ion-acoustic solitons have scale sizes of ~10 Debye lengths both parallel and perpendicular to the magnetic field, and amplitude $\frac{e\phi}{T_e} \sim 0.1$. The speeds, scale lengths, and amplitudes of the ion-acoustic solitons were found to be consistent with the ESWs observed by Polar.[37,225]

Lu *et al.*[228] performed 1D electrostatic particle simulations of ESWs in a plasma composed of three electron components, namely, cold, hot, and beam electrons and immobile ions providing a neutralizing background. Initially, electron-acoustic waves are excited, grow in amplitude, and trap a part of hot and beam electrons forming phase-space electron holes. These waves coalesce with each other and nonlinearly evolve into solitary structures. The structures are stable electron acoustic solitons with positive potentials, bipolar electric fields, scale sizes of ~200 cold electron Debye lengths, propagation speeds related to bulk velocity of beam electrons, and are associated with cold electron density cavities. The properties of the simulated electron-acoustic solitons seem to be in good agreement with that of the ESWs observed in the auroral region by Polar and FAST satellites.[15,26,29,31,34] Shukla *et al.*[229] have investigated the nonlinear evolution of electron-acoustic waves in a magnetized plasma consisting of cold electrons, beam electrons, and hot electrons having vortex-like distribution (i.e., electron phase space holes) and immobile ions. The evolution of 3D electron-acoustic solitary waves is described by the modified KdV equation. The numerical solution of the modified KdV equation show ESWs having positive potential with corresponding dip (hump) in cold (hot) electron number density. Recently, Vasko[51] and Dillard *et al.*[230] have provided the direct identification of the ESWs observed by Van Allen probe in terms of electron-acoustic solitons and double layers (DL).

In view of the above, it seems that ion- and electron-acoustic solitary wave models have an edge over the phase-space hole models. From the PIC simulations of ion- and electron-acoustic solitary waves[137,190,193–195,224,228] and theoretical analysis by Shukla *et al.*,[229] it is clear that the formation of ion and electron phase-space holes is an intermediate process to get rid of free energy in the system, and in the final nonlinear evolution stage, the ion and electron solitary waves are produced. In a multi-component plasma, as discussed here, one can have slow ion acoustic solitons with either positive and negative potential, fast ion-acoustic solitons with positive potential, and electron-acoustic solitons with positive potential. However, electron-acoustic solitons can also have a negative potential, as shown in earlier models.[13,14,91,92,95,96,109–113,144–146] Further, the amplitudes of ion- and electron-acoustic solitons described by the Sagdeev pseudo-potential theory can either increase or decrease with increase in their widths depending upon the plasma parameters. Therefore, the prevailing objections against the soliton models cannot be sustained. As stated above, it would be worthwhile to study 2D and 3D ion- and electron-acoustic solitons in magnetized plasmas to bring the predictions of the soliton models closer to the ESWs observations in space.

ACKNOWLEDGMENTS

G.S.L. is thankful to the Indian National Science Academy (INSA), New Delhi, for the support under the INSA Honorary Scientist scheme.

[1]D. A. Gurnett, R. R. Anderson, B. T. Tsurutani, E. J. Smith, G. Paschmann, G. Haerendel, S. J. Bame, and C. T. Russell, J. Geophys. Res. **84**(A12), 7043–7058, https://doi.org/10.1029/JA084iA12p07043 (1979).
[2]F. L. Scarf, L. A. Frank, K. L. Ackerson, and R. P. Lepping, Geophys. Res. Lett. **1**, 189–192, https://doi.org/10.1029/GL001i005p00189 (1974).
[3]D. A. Gurnett, L. A. Frank, and R. P. Lepping, J. Geophys. Res. **81**, 6059–6071, https://doi.org/10.1029/JA081i034p06059 (1976).
[4]D. A. Gurnett and L. A. Frank, J. Geophys. Res. **82**, 1031–1050, https://doi.org/10.1029/JA082i007p01031 (1977).
[5]C. A. Cattell, F. S. Mozer, R. R. Anderson, E. W. Hones, and R. D. Sharp, J. Geophys. Res. **91**, 5681–5688, https://doi.org/10.1029/JA091iA05p05681 (1986).
[6]B. T. Tsurutani, G. S. Lakhina, C. M. Ho, J. K. Arballo, C. Galvan, A. Boonsiriseth, J. S. Pickett, D. A. Gurnett, W. K. Peterson, and R. M. Thorne, J. Geophys. Res. **103(A8)**, 17351–17366, https://dx.doi.org/10.1029/97JA03063 (1998).
[7]P. Rodriguez and D. A. Gurnett, J. Geophys. Res. **80**, 19–31, https://doi.org/10.1029/JA080i001p00019 (1975).
[8]T. G. Onsager, R. H. Holzworth, H. C. Koons, O. H. Bauer, D. A. Gurnett, R. R. Anderson, H. Lühr, and C. W. Carlson, J. Geophys. Res. **94**, 13397–13408, https://doi.org/10.1029/JA094iA10p13397 (1989).

[9]R. R. Anderson, C. C. Harvey, M. M. Hoppe, B. T. Tsurutani, T. E. Eastman, and J. Etcheto, J. Geophys. Res. **87**, 2087–2107, https://doi.org/10.1029/JA087iA04p02087 (1982).
[10]J. S. Pickett, L.-J. Chen, S. W. Kahler, O. Santolík, M. L. Goldstein, B. Lavraud, P. M. E. Décréau, R. Kessel, E. Lucek, G. S. Lakhina, B. T. Tsurutani, D. A. Gurnett, N. Cornilleau-Wehrlin, A. Fazakerley, H. Rème, and A. Balogh, Nonlinear Process. Geophys. **12**, 181–193 (2005).
[11]F. L. Scarf, R. W. Fredricks, I. M. Green, and C. T. Russell, J. Geophys. Res. **77**, 2274–2293, https://doi.org/10.1029/JA077i013p02274 (1972).
[12]D. A. Gurnett and L. A. Frank, J. Geophys. Res. **83**, 1447–1462, https://doi.org/10.1029/JA083iA04p01447 (1978).
[13]R. Pottelette, M. Malingre, N. Dubouloz, B. Aparicio, R. Lundin, G. Holmgren, and G. Marklund, J. Geophys. Res. **95**, 5957–5971, https://doi.org/10.1029/JA095iA05p05957 (1990).
[14]N. Dubouloz, R. Pottelette, M. Malingre, G. Holmgren, and P. A. Lindqvist, J. Geophys. Res. **96**, 3565–3579, https://doi.org/10.1029/90JA02355 (1991).
[15]R. E. Ergun, C. W. Carlson, J. P. McFadden, F. S. Mozer, G. T. Delory, W. Peria, C. C. Chaston, M. Temerin, I. Roth, L. Muschietti, R. Elphic, R. Strangeway, R. Pfaff, C. A. Cattell, D. Klumpar, E. Shelley, W. Peterson, E. Moebius, and L. Kistler, Geophys. Res. Lett. **25**, 2041–2044, https://doi.org/10.1029/98GL00636 (1998).
[16]J. P. McFadden, C. W. Carlson, and R. E. Ergun, J. Geophys. Res. **104**, 14453–14480, https://doi.org/10.1029/1998JA900167 (1999).
[17]T. E. Eastman, L. A. Frank, W. K. Peterson, and W. Lennartsson, J. Geophys. Res. **89**, 1553–1572, https://doi.org/10.1029/JA089iA03p01553 (1984).
[18]G. S. Lakhina, B. T. Tsurutani, H. Kojima, and H. Matsumoto, J. Geophys. Res. **105**, 27791–27831, https://doi.org/10.1029/2000JA900054 (2000).
[19]B. T. Tsurutani, E. J. Smith, R. M. Thorne, R. R. Anderson, D. A. Gurnett, G. K. Parks, C. S. Lin, and C. T. Russell, Geophys. Res. Lett. **8**, 183–186, https://doi.org/10.1029/GL008i002p00183 (1981).
[20]M. Temerin, K. Cerny, W. Lotko, and F. S. Mozer, Phys. Rev. Lett. **48**, 1175–1179 (1982).
[21]R. Boström, G. Gustafsson, B. Holback, G. Holmgren, H. Koskinen, and P. Kintner, Phys. Rev. Lett. **61**, 82–85 (1988).
[22]H. E. J. Koskinen, R. Lundin, and B. Holback, J. Geophys. Res. **95**, 5921–5929, https://doi.org/10.1029/JA095iA05p05921 (1990).
[23]H. Matsumoto, H. Kojima, T. Miyatake, Y. Omura, M. Okada, I. Nagano, and M. Tsutsui, Geophys. Res. Lett. **21**, 2915–2918, https://doi.org/10.1029/94GL01284 (1994).
[24]H. Kojima, H. Matsumoto, and Y. Omura, Adv. Space Res. **23**, 1689–1697 (1999).
[25]G. S. Lakhina, B. T. Tsurutani, and J. S. Pickett, Nonlinear Process. Geophys. **11**, 205–213 (2004).
[26]J. R. Franz, P. M. Kintner, and J. S. Pickett, Geophys. Res. Lett. **25**, 1277–1280, https://doi.org/10.1029/98GL50870 (1998).
[27]C. Cattell, J. Wygant, J. Dombeck, F. S. Mozer, M. Temerin, and C. T. Russell, Geophys. Res. Lett. **25**, 857–860, https://doi.org/10.1029/98GL00497 (1998).
[28]C. Cattell, R. Bergmann, K. Sigsbee, C. Carlson, C. Chaston, R. Ergun, J. McFadden, F. S. Mozer, M. Temerin, R. Strangeway, R. Elphic, L. Kistler, E. Moebius, L. Tang, D. Klumpar, and R. Pfaff, Geophys. Res. Lett. **25**, 2053–2056, https://doi.org/10.1029/98GL00834 (1998).
[29]C. A. Cattell, J. Dombeck, J. R. Wygant, M. K. Hudson, F. S. Mozer, M. A. Temerin, W. K. Peterson, C. A. Kletzing, C. T. Russell, and R. F. Pfaff, Geophys. Res. Lett. **26**, 425–428, https://doi.org/10.1029/1998GL900304 (1999).
[30]C. Cattell, J. Dombeck, J. Wygant, J. F. Drake, M. Swisdak, M. L. Goldstein, W. Keith, A. Fazakerley, M. André, E. Lucek, and A. Balogh, J. Geophys. Res. **110**, A01211, https://dx.doi.org/10.1029/2004JA010519 (2005).
[31]B. T. Tsurutani, J. K. Arballo, G. S. Lakhina, C. M. Ho, B. Buti, J. S. Pickett, and D. A. Gurnett, Geophys. Res. Lett. **25**, 4117–4120, https://doi.org/10.1029/1998GL900114 (1998).
[32]J. S. Pickett, D. A. Gurnett, J. D. Menietti, M. J. LeDocq, J. D. Scudder, L. A. Frank, J. B. Sigwarth, K. L. Ackerson, D. D. Morgan, P. M. Franz, J. R. Kintner, B. T. Tsurutani, C. M. Ho, J. Chen, T. A. Fritz, C. T. Russell, W. K. Peterson, Y. Kasahara, I. Kimura, S. Watanabe, G. G. Arkos, G. Rostoker, S. Kokubun, H. Fukunishi, R. F. Pfaff, F. S. Mozer, S. Y. Hsieh, T. Mukai, and M. O. Chandler, Adv. Space Res. **24**, 23–33 (1999).
[33]J. S. Pickett, J. D. Menietti, J. H. Dowell, D. A. Gurnett, and J. D. Scudder, Nonlinear Process. Geophys. **6**, 195–204 (1999).
[34]F. S. Mozer, R. Ergun, M. Temerin, C. Cattell, J. Dombeck, and J. Wygant, Phys. Rev. Lett. **79**, 1281–1284 (1997).
[35]R. E. Ergun, C. W. Carlson, J. P. McFadden, F. S. Mozer, L. Muschietti, I. Roth, and R. J. Strangeway, Phys. Rev. Lett. **81**, 826–829 (1998).
[36]R. E. Ergun, C. W. Carlson, L. Muschietti, I. Roth, and J. P. McFadden, Nonlinear Process. Geophys. **6**, 187–194 (1999).
[37]S. R. Bounds, R. F. Pfaff, S. F. Knowlton, F. S. Mozer, M. A. Temerin, and C. A. Kletzing, J. Geophys. Res. **104**, 28709–28717, https://doi.org/10.1029/1999JA900284 (1999).
[38]H. Kojima, H. Matsumoto, S. Chikuba, S. Horiyama, M. Ashour-Abdalla, and R. R. Anderson, J. Geophys. Res. **102**, 14439–14455, https://doi.org/10.1029/97JA00684 (1997).
[39]J. S. Pickett, J. D. Menietti, D. A. Gurnett, B. Tsurutani, P. M. Kintner, E. Klatt, and A. Balogh, Nonlinear Process. Geophys. **10**, 3–11 (2003).
[40]J. S. Pickett, L.-J. Chen, S. W. Kahler, O. Santolík, D. A. Gurnett, B. T. Tsurutani, and A. Balogh, Ann. Geophys. **22**, 2515–2523 (2004).
[41]L. Andersson, R. E. Ergun, J. Tao, A. Roux, O. LeContel, V. Angelopoulos, J. Bonnell, J. P. McFadden, D. E. Larson, S. Eriksson, T. Johansson, C. M. Cully, D. L. Newman, M. V. Goldman, K.-H. Glassmeier, and W. Baumjohann, Phys. Rev. Lett. **102**, 225004 (2009).
[42]H. Matsumoto, X. H. Deng, H. Kojima, and R. R. Anderson, Geophys. Res. Lett. **30**, 1326, https://dx.doi.org/10.1029/2002GL016319 (2003).
[43]X. H. Deng, H. Matsumoto, H. Kojima, T. Mukai, R. R. Anderson, W. Baumjohann, and R. Nakamura, J. Geophys. Res. **109**, A05206, https://doi.org/10.1029/2003JA010031 (2004).
[44]X. H. Deng, R. X. Tang, H. Matsumoto, J. S. Pickett, A. N. Fazakerley, H. Kojima, W. Baumjohann, A. Coates, R. Nakamura, D. A. Gurnett, and Z. X. Liu, Adv. Space Res. **37**, 1373–1381 (2006).
[45]S. Li, X. Deng, M. Zhou, R. Tang, K. Liu, H. Kojima, and H. Matsumoto, Adv. Space Res. **43**, 394–400 (2009).
[46]S. Li, S. Zhang, H. Cai, and H. Yang, Earth Planets Space **67**, 84 (2015).
[47]S. D. Bale, P. J. Kellogg, D. E. Larsen, R. P. Lin, K. Goetz, and R. P. Lepping, Geophys. Res. Lett. **25**, 2929–2932, https://doi.org/10.1029/98GL02111 (1998).
[48]R. Behlke, M. Andrè, S. D. Bale, J. S. Pickett, C. A. Cattell, E. A. Lucek, and A. Balogh, Geophys. Res. Lett. **31**, L16805, https://doi.org/10.1029/2004GL019524 (2004).
[49]S. Y. Li, S. F. Zhang, H. Cai, X. H. Deng, X. Q. Chen, M. Zhou, and H. B. Yang, Geophys. Res. Lett. **40**, 3356–3361, https://doi.org/10.1002/grl.50623 (2013).
[50]F. S. Mozer, O. V. Agapitov, A. Artemyev, J. F. Drake, V. Krasnoselskikh, S. Lejosne, and I. Vasko, Geophys. Res. Lett. **42**, 3627–3638, https://doi.org/10.1002/2015GL063946 (2015).
[51]I. Y. Vasko, O. V. Agapitov, F. S. Mozer, J. W. Bonnell, A. V. Artemyev, V. V. Krasnoselskikh, G. Reeves, and G. Hospodarsky, Geophys. Res. Lett. **44**, 4575–4583, https://doi.org/10.1002/2017GL074026 (2017).
[52]A. Mangeney, C. Salem, C. Lacombe, J.-L. Bougeret, C. Perche, R. Manning, P. J. Kellogg, K. Goetz, S. J. Monson, and J.-M. Bosqued, Ann. Geophys. **17**, 307–320 (1999).
[53]D. M. Malaspina, D. L. Newman, L. B. Willson, K. Goetz, P. J. Kellogg, and K. Kerstin, J. Geophys. Res. **118**, 591–599, https://doi.org/10.1002/jgra.50102 (2013).
[54]K. Hashimoto, M. Hashitani, Y. Kasahara, Y. Omura, M. N. Nishino, Y. Saito, S. Yokota, T. Ono, H. Tsunakawa, H. Shibuya, M. Matsushima, H. Shimizu, and F. Takahashi, Geophys. Res. Lett. **37**, L19204, https://dx.doi.org/10.1029/2010GL044529 (2010).
[55]Y. Omura, H. Kojima, N. Miki, T. Mukai, H. Matsumoto, and R. Anderson, J. Geophys. Res. **104**, 14627–14637, https://doi.org/10.1029/1999JA900103 (1999).
[56]J. R. Franz, P. M. Kintner, J. S. Pickett, and L.-J. Chen, J. Geophys. Res. **110**, A09212, https://dx.doi.org/10.1029/2005JA011095 (2005).
[57]C. Norgren, M. André, A. Vaivads, and Y. V. Khotyaintsev, Geophys. Res. Lett. **42**, 1654–1661, https://doi.org/10.1002/2015GL063218 (2015).
[58]J. R. Franz, P. M. Kintner, C. E. Seyler, J. S. Pickett, and J. D. Scudder, Geophys. Res. Lett. **27**, 169–172, https://doi.org/10.1029/1999GL010733 (2000).
[59]I. B. Bernstein, J. M. Greene, and M. D. Kruskal, Phys. Rev. **108**, 546–550 (1957).
[60]H. Schamel, Phys. Scr. **T2/1**, 228 (1982).
[61]H. Schamel, Phys. Plasmas **7**, 4831–4844 (2000).
[62]H. Schamel, Phys. Plasmas **22**, 042301 (2015).
[63]Y. Omura, H. Matsumoto, T. Miyake, and H. Kojima, J. Geophys. Res. **101**, 2685–2697, https://doi.org/10.1029/95JA03145 (1996).

[64]M. V. Goldman, M. M. Oppenheim, and D. L. Newman, Geophys. Res. Lett. **26**, 1821–1824, https://doi.org/10.1029/1999GL900435 (1999).
[65]M. Oppenheim, D. L. Newman, and M. V. Goldman, Phys. Rev. Lett. **83**, 2344–2347 (1999).
[66]L. Muschietti, R. E. Ergun, I. Roth, and C. W. Carlson, Geophys. Res. Lett. **26**, 1093–1096, https://doi.org/10.1029/1999GL900207 (1999).
[67]N. Singh, Nonlinear Process. Geophys. **10**, 53–63 (2003).
[68]L.-J. Chen, J. Pickett, P. Kintner, J. Franz, and D. Gurnett, J. Geophys. Res. **110**, A09211, https://doi.org/10.1029/2005JA011087 (2005).
[69]Y. Omura, H. Kojima, and H. Matsumoto, Geophys. Res. Lett. **21**, 2923–2926, https://doi.org/10.1029/94GL01605 (1994).
[70]I. H. Hutchinson, Phys. Plasmas **24**, 055601 (2017).
[71]N. Singh and R. W. Schunk, Plasma Phys. Controlled Fusion **26**, 859 (1984).
[72]N. Singh, H. Thiemann, and R. W. Schunk, Planet. Space Sci. **35**, 353–395 (1987).
[73]N. Singh, S. M. Loo, and E. Wells, J. Geophys. Res. **106**, 21183–21198, https://doi.org/10.1029/2001JA900056 (2001).
[74]N. Singh and G. Khazanov, J. Geophys. Res. **108**, 8007, https://doi.org/10.1029/2002JA009436 (2003).
[75]L. Muschietti, I. Roth, C. W. Carlson, and R. E. Ergun, Phys. Rev. Lett. **85**, 94–97 (2000).
[76]D. Jovanović and P. K. Shukla, Phys. Rev. Lett. **84**, 4373–4376 (2000).
[77]D. Jovanović, P. K. Shukla, L. Stenflo, and F. Pegoraro, J. Geophys. Res. **107**, SMP 15–1–SMP 15–6, https://doi.org/10.1029/2001JA900180 (2002).
[78]D. Jovanović and P. K. Shukla, Geophys. Res. Lett. **31**, L15802, https://doi.org/10.1029/2003GL018047 (2004).
[79]D. Jovanović, P. K. Shukla, and G. Morfill, Phys. Plasmas **12**, 112903 (2005).
[80]D. Jovanović, P. K. Shukla, and G. E. Morfill, J. Geophys. Res. **111**, 3210, https://dx.doi.org/10.1029/2005JA011227 (2006).
[81]D. Jovanović, P. K. Shukla, and G. Morfill, Phys. Plasmas **14**, 082901 (2007).
[82]D. Jovanović, P. K. Shukla, and H. Schamel, Phys. Plasmas **7**, 3247–3251 (2000).
[83]D. Jovanović and P. K. Shukla, Phys. Rev. Lett. **90**, 135001 (2003).
[84]D. Jovanović, P. K. Shukla, and G. Morfill, J. Plasma Phys. **71**, 203–211 (2005).
[85]J. S. Pickett, S. W. Kahler, L.-J. Chen, R. L. Huff, O. Santolík, Y. Khotyaintsev, P. M. E. Décréau, D. Winningham, R. Frahm, M. L. Goldstein, G. S. Lakhina, B. T. Tsurutani, B. Lavraud, D. A. Gurnett, M. André, A. Fazakerley, A. Balogh, and H. Rème, Nonlinear Process. Geophys. **11**, 183–196 (2004).
[86]D. Jovanović and V. V. Krasnoselskikh, Phys. Plasmas **16**, 102902 (2009).
[87]A. J. Hull, D. E. Larson, M. Wilber, J. D. Scudder, F. S. Mozer, C. T. Russell, and S. D. Bale, Geophys. Res. Lett. **33**, L15104, https://doi.org/10.1029/2005GL025564 (2006).
[88]Y. Hobara, S. N. Walker, M. Balikhin, O. A. Pokhotelov, M. Gedalin, V. Krasnoselskikh, M. Hayakawa, M. André, M. Dunlop, H. Rème, and A. Fazakerley, J. Geophys. Res. **113**, A05211, https://dx.doi.org/10.1029/2007JA012789 (2008).
[89]R. Z. Sagdeeev, Rev. Plasma Phys. **4**, 23 (1966).
[90]S. S. Ghosh and G. S. Lakhina, Nonlinear Process. Geophys. **11**, 219–228 (2004).
[91]S. V. Singh, R. V. Reddy, and G. S. Lakhina, Adv. Space Res. **28**, 1643–1648 (2001).
[92]S. V. Singh and G. S. Lakhina, Nonlinear Process. Geophys. **11**, 275–279 (2004).
[93]A. P. Kakad, S. V. Singh, R. V. Reddy, G. S. Lakhina, S. G. Tagare, and F. Verheest, Phys. Plasmas **14**, 052305 (2007).
[94]S. S. Ghosh, J. S. Pickett, G. S. Lakhina, J. D. Winningham, B. Lavraud, and P. M. E. Décréau, J. Geophys. Res. **113**, A06218, https://dx.doi.org/10.1029/2007JA012768 (2008).
[95]G. S. Lakhina, A. P. Kakad, S. V. Singh, and F. Verheest, Phys. Plasmas **15**, 062903 (2008).
[96]G. S. Lakhina, S. V. Singh, A. P. Kakad, F. Verheest, and R. Bharuthram, Nonlinear Process. Geophys. **15**, 903–913 (2008).
[97]G. S. Lakhina, S. V. Singh, A. P. Kakad, M. L. Goldstein, A. F. Viñas, and J. S. Pickett, J. Geophys. Res. **114**, A09212, https://doi.org/10.1029/2009JA014306 (2009).
[98]G. S. Lakhina, S. V. Singh, and A. P. Kakad, Adv. Space Res. **47**, 1558–1567 (2011).
[99]G. S. Lakhina, S. V. Singh, A. P. Kakad, and J. S. Pickett, J. Geophys. Res. **116**, A10218, https://dx.doi.org/10.1029/2011JA016700 (2011).
[100]S. K. Maharaj, R. Bharuthram, S. Singh, and G. Lakhina, Phys. Plasmas **19**, 122301 (2012).
[101]M. V. Goldman, D. L. Newman, and A. Mangeney, Phys. Rev. Lett. **99**, 145002 (2007).
[102]J. B. Tao, R. E. Ergun, L. Andersson, J. W. Bonnell, A. Roux, O. LeContel, V. Angelopoulos, J. P. McFadden, D. E. Larson, C. M. Cully, H.-U. Auster, K.-H. Glassmeier, W. Baumjohann, D. L. Newman, and M. V. Goldman, J. Geophys. Res. **116**, A11213, https://doi.org/10.1029/2010JA016054 (2011).
[103]B. Buti, Phys. Lett. A **76**, 251–254 (1980).
[104]M. Y. Yu, P. K. Shukla, and S. Bujarbarua, Phys. Fluids **23**, 2146–2147 (1980).
[105]M. K. Hudson, W. Lotko, I. Roth, and E. Witt, J. Geophys. Res. **88**, 916–926, https://doi.org/10.1029/JA088iA02p00916 (1983).
[106]S. Qian, W. Lotko, and M. K. Hudson, Phys. Fluids **31**, 2190–2200 (1988).
[107]R. V. Reddy and G. S. Lakhina, Planet. Space Sci. **39**, 1343–1350 (1991).
[108]R. V. Reddy, G. Lakhina, and F. Verheest, Planet. Space Sci. **40**, 1055–1062 (1992).
[109]M. Berthomier, R. Pottelette, and M. Malingre, J. Geophys. Res. **103**, 4261–4270, https://doi.org/10.1029/97JA00338 (1998).
[110]R. L. Mace, S. Baboolal, R. Bharuthram, and M. A. Hellberg, J. Plasma Phys. **45**, 323–338 (1991).
[111]N. Dubouloz, R. A. Treumann, R. Pottelette, and M. Malingre, J. Geophys. Res. **98**, 17415–17422, https://doi.org/10.1029/93JA01611 (1993).
[112]N. Dubouloz, R. Pottelette, M. Malingre, and R. A. Treumann, Geophys. Res. Lett. **18**, 155–158, https://doi.org/10.1029/90GL02677 (1991).
[113]S. G. Tagare, S. V. Singh, R. V. Reddy, and G. S. Lakhina, Nonlinear Process. Geophys. **11**, 215–218 (2004).
[114]M. Berthomier, R. Pottelette, M. Malingre, and Y. Khotyaintsev, Phys. Plasmas **7**, 2987–2994 (2000).
[115]M. Berthomier, R. Pottelette, L. Muschietti, I. Roth, and C. W. Carlson, Geophys. Res. Lett. **30**, 2148, https://dx.doi.org/10.1029/2003GL018491 (2003).
[116]G. S. Lakhina, B. T. Tsurutani, S. V. Singh, and R. V. Reddy, Nonlinear Process. Geophys. **10**, 65–73 (2003).
[117]F. Verheest, T. Cattaert, and M. A. Hellberg, Space Sci. Rev. **121**, 299–311 (2005).
[118]T. Cattaert, F. Verheest, and M. A. Hellberg, Phys. Plasmas **12**, 042901 (2005).
[119]S. V. Singh, G. S. Lakhina, R. Bharuthram, and S. R. Pillay, Phys. Plasmas **18**, 122306 (2011).
[120]A. Teste and G. K. Parks, Phys. Rev. Lett. **102**, 075003 (2009).
[121]H. Washimi and T. Taniuti, Phys. Rev. Lett. **17**, 996–998 (1966).
[122]M. Q. Tran, Phys. Scr. **20**, 317 (1979).
[123]G. Chanteur and M. Raadu, Phys. Fluids **30**, 2708–2719 (1987).
[124]S. Baboolal, R. Bharuthram, and M. A. Hellberg, J. Plasma Phys. **44**, 1–23 (1990).
[125]S. S. Ghosh, K. K. Ghosh, and A. N. S. Iyengar, Phys. Plasmas **3**, 3939–3946 (1996).
[126]S. S. Ghosh and A. N. S. Iyengar, Phys. Plasmas **4**, 3204–3210 (1997).
[127]S. K. Maharaj, R. Bharuthram, S. V. Singh, and G. S. Lakhina, Phys. Plasmas **19**, 072320 (2012).
[128]S. V. Singh, S. Devanandhan, G. S. Lakhina, and R. Bharuthram, Phys. Plasmas **20**, 012306 (2013).
[129]O. R. Rufai, R. Bharuthram, S. V. Singh, and G. S. Lakhina, Phys. Plasmas **19**, 122308 (2012).
[130]O. R. Rufai, R. Bharuthram, S. V. Singh, and G. S. Lakhina, Commun. Nonlinear Sci. Numer. Simul. **19**, 1338–1346 (2014).
[131]O. R. Rufai, R. Bharuthram, S. V. Singh, and G. S. Lakhina, Phys. Plasmas **21**, 082304 (2014).
[132]S. V. Singh and G. S. Lakhina, Commun. Nonlinear Sci. Numer. Simul. **23**, 274–281 (2015).
[133]S. K. Maharaj, R. Bharuthram, S. V. Singh, and G. S. Lakhina, Phys. Plasmas **22**, 032313 (2015).
[134]O. R. Rufai, R. Bharuthram, S. V. Singh, and G. S. Lakhina, Phys. Plasmas **22**, 102305 (2015).
[135]O. R. Rufai, R. Bharuthram, S. V. Singh, and G. S. Lakhina, Adv. Space Res. **57**, 813–820 (2016).

[136]O. R. Rufai, R. Bharuthram, S. V. Singh, and G. S. Lakhina, Phys. Plasmas **23**, 032309 (2016).
[137]A. Kakad, B. Kakad, C. Anekallu, G. Lakhina, Y. Omura, and A. Fazakerley, J. Geophys. Res. **121**, 4452–4465, https://doi.org/10.1002/2016JA022365 (2016).
[138]R. Pottelette, R. E. Ergun, R. A. Treumann, M. Berthomier, C. W. Carlson, J. P. McFadden, and I. Roth, Geophys. Res. Lett. **26**, 2629–2632, https://doi.org/10.1029/1999GL900462 (1999).
[139]S. V. Singh and G. S. Lakhina, Planet. Space Sci. **49**, 107–114 (2001).
[140]A. P. Kakad, S. V. Singh, R. V. Reddy, G. S. Lakhina, and S. G. Tagare, Adv. Space Res. **43**, 1945–1949 (2009).
[141]L. N. Mbuli, S. K. Maharaj, R. Bharuthram, S. V. Singh, and G. S. Lakhina, Phys. Plasmas **22**, 062307 (2015).
[142]L. N. Mbuli, S. K. Maharaj, R. Bharuthram, S. V. Singh, and G. S. Lakhina, Phys. Plasmas **23**, 062302 (2016).
[143]S. V. Singh, S. Devanandhan, G. S. Lakhina, and R. Bharuthram, Phys. Plasmas **23**, 082310 (2016).
[144]B. Buti, M. Mohan, and P. K. Shukla, J. Plasma Phys. **23**, 341–347 (1980).
[145]B. Buti, J. Plasma Phys. **24**, 169–180 (1980).
[146]M. Mohan and B. Buti, Plasma Phys. **22**, 873 (1980).
[147]V. M. Vasyliunas, J. Geophys. Res. **73**, 2839–2884, https://doi.org/10.1029/JA073i009p02839 (1968).
[148]M. P. Leubner, J. Geophys. Res. **87**, 6335–6338, https://doi.org/10.1029/JA087iA08p06335 (1982).
[149]E. Marsch, K.-H. Mühlhäuser, H. Rosenbauer, R. Schwenn, and F. M. Neubauer, J. Geophys. Res. **87**, 35–51, https://doi.org/10.1029/JA087iA01p00035 (1982).
[150]T. P. Armstrong, M. T. Paonessa, E. V. Bell, and S. M. Krimigis, J. Geophys. Res. **88**, 8893–8904, https://doi.org/10.1029/JA088iA11p08893 (1983).
[151]M. P. Leubner, Planet. Space Sci. **48**, 133–141 (2000).
[152]D. Summers and R. M. Thorne, Phys. Fluids B **3**, 1835–1847 (1991).
[153]R. M. Thorne and D. Summers, Phys. Fluids B **3**, 2117–2123 (1991).
[154]R. M. Thorne and D. Summers, J. Geophys. Res. **96**, 217–223, https://doi.org/10.1029/90JA01629 (1991).
[155]R. M. Thorne and R. B. Horne, J. Geophys. Res. **99**, 17249–17258, https://doi.org/10.1029/94JA01006 (1994).
[156]R. L. Mace and M. A. Hellberg, Phys. Plasmas **2**, 2098–2109 (1995).
[157]M. A. Hellberg and R. L. Mace, Phys. Plasmas **9**, 1495–1504 (2002).
[158]M. Hapgood, C. Perry, J. Davies, and M. Denton, Planet. Space Sci. **59**, 618–629 (2011).
[159]G. Livadiotis and D. J. McComas, J. Geophys. Res. **114**, A11105, https://doi.org/10.1029/2009JA014352 (2009).
[160]G. Livadiotis and D. J. McComas, J. Plasma Phys. **80**, 341–378 (2014).
[161]V. Pierrard and M. Lazar, Sol. Phys. **267**, 153–174 (2010).
[162]G. Livadiotis, J. Geophys. Res. **120**, 1607–1619, https://doi.org/10.1002/2014JA020825 (2015).
[163]G. Livadiotis, J. Geophys. Res. **120**, 880–903, https://doi.org/10.1002/2014JA020671 (2015).
[164]N. S. Saini, I. Kourakis, and M. A. Hellberg, Phys. Plasmas **16**, 062903 (2009).
[165]N. S. Saini and I. Kourakis, Plasma Phys. Controlled Fusion **52**, 075009 (2010).
[166]S. Devanandhan, S. V. Singh, and G. S. Lakhina, Phys. Scr. **84**, 025507 (2011).
[167]S. Devanandhan, S. V. Singh, G. S. Lakhina, and R. Bharuthram, Nonlinear Process. Geophys. **18**, 627–634 (2011).
[168]S. Devanandhan, S. V. Singh, G. S. Lakhina, and R. Bharuthram, Phys. Plasmas **19**, 082314 (2012).
[169]S. Devanandhan, S. V. Singh, G. S. Lakhina, and R. Bharuthram, Commun. Nonlinear Sci. Numer. Simul. **22**, 1322–1330 (2015).
[170]G. S. Lakhina and S. V. Singh, Sol. Phys. **290**, 3033–3049 (2015).
[171]R. Rubia, S. V. Singh, and G. S. Lakhina, Phys. Plasmas **23**, 062902 (2016).
[172]G. S. Lakhina and S. V. Singh, "Solitary waves in plasmas described by kappa distributions," in *Kappa Distributions*, edited by G. Livadiotis (Elsevier, 2017), Chap. 9, pp. 399–418.
[173]R. Rubia, S. V. Singh, and G. S. Lakhina, J. Geophys. Res. Space Phys. **122**, 9134–9147 (2017).
[174]R. Rubia, S. V. Singh, and G. S. Lakhina, Phys. Plasmas **25**, 032302 (2018).
[175]T. K. Baluku, M. A. Hellberg, and F. Verheest, Europhys. Lett. **91**, 15001 (2010).
[176]G. S. Lakhina, S. V. Singh, and A. P. Kakad, Phys. Plasmas **21**, 062311 (2014).
[177]J. E. Borovsky and S. P. Gary, J. Geophys. Res. **119**, 5210, https://doi.org/10.1002/2014JA019758 (2014).
[178]S. Bourouaine, E. Marsch, and F. M. Neubauer, Astrophys. J. Lett. **728**, L3 (2011).
[179]M. Maksimovic, V. Pierrard, and P. Riley, Geophys. Res. Lett. **24**, 1151–1154, https://doi.org/10.1029/97GL00992 (1997).
[180]J. B. Tao, R. E. Ergun, D. L. Newman, J. S. Halekas, L. Andersson, V. Angelopoulos, J. W. Bonnell, J. P. McFadden, C. M. Cully, H.-U. Auster, K.-H. Glassmeier, D. E. Larson, W. Baumjohann, and M. V. Goldman, J. Geophys. Res. **117**, A03106, https://doi.org/10.1029/2011JA017364 (2012).
[181]C. Lacombe, C. Salem, A. Mangeney, D. Hubert, C. Perche, J.-L. Bougeret, P. J. Kellogg, and J.-M. Bosqued, Ann. Geophys. **20**, 609–618 (2002).
[182]C. Salem, C. Lacombe, A. Mangeney, P. J. Kellogg, and J. Bougeret, AIP Conf. Proc. **6**, 513–517 (2003).
[183]K. W. Ogilvie, J. T. Steinberg, R. J. Fitzenreiter, C. J. Owen, A. J. Lazarus, W. M. Farrell, and R. B. Torbert, Geophys. Res. Lett. **23**, 1255–1258, https://doi.org/10.1029/96GL01069 (1996).
[184]S. Wiehle, F. Plaschke, U. Motschmann, K. H. Glassmeier, H. U. Auster, V. Angelopoulos, J. Mueller, H. Kriegel, E. Georgescu, J. Halekas, and D. Sibeck, Planet. Space Sci. **59**, 661–671 (2011).
[185]W. M. Farrell, M. L. Kaiser, J. Steinberg, and S. D. Bale, J. Geophys. Res. **103**, 23653–23660, https://doi.org/10.1029/97JA03717 (1998).
[186]P. C. Birch and S. C. Chapman, Geophys. Res. Lett. **28**, 219–222, https://doi.org/10.1029/2000GL011958 (2001).
[187]P. C. Birch and S. C. Chapman, Phys. Plasmas **9**, 1785–1789 (2002).
[188]W. S. Kurth, D. A. Gurnett, A. M. Persoon, A. Roux, S. J. Bolton, and C. J. Alexander, Planet. Space Sci. **49**, 345–363 (2001).
[189]J. D. Williams, L.-J. Chen, W. S. Kurth, D. A. Gurnett, M. K. Dougherty, and A. M. Rymer, Geophys. Res. Lett. **32**, L17103, https://doi.org/10.1029/2005GL023079 (2005).
[190]A. Kakad, Y. Omura, and B. Kakad, Phys. Plasmas **20**, 062103 (2013).
[191]A. Lotekar, A. Kakad, and B. Kakad, Phys. Plasmas **23**, 102108 (2016).
[192]A. Lotekar, A. Kakad, and B. Kakad, Phys. Plasmas **24**, 102127 (2017).
[193]B. Kakad, A. Kakad, and Y. Omura, J. Geophys. Res. **119**, 5589–5599, https://doi.org/10.1002/2014JA019798 (2014).
[194]B. Kakad, A. Kakad, and Y. Omura, Phys. Plasmas **24**, 102122 (2017).
[195]A. Kakad, B. Kakad, and Y. Omura, Phys. Plasmas **24**, 060704 (2017).
[196]A. Davey and K. Stewartson, Proc. R. Soc. London **338A**, 101–110 (1974).
[197]S. S. Ghosh, A. Sen, and G. S. Lakhina, Pramana **55**, 693–698 (2000).
[198]S. S. Ghosh, A. Sen, and G. S. Lakhina, Nonlinear Process. Geophys. **9**, 463–475 (2002).
[199]K. H. Spatschek, P. Shukla, and M. Yu, Phys. Lett. A **54**, 419–420 (1975).
[200]B. B. Kadomtsev and V. I. Petviashvili, Sov. Phys. Dokl. **15**, 539–541 (1970).
[201]E. A. Kuznetsov and S. K. Turitsyn, Sov. Phys. JETP **55**, 844–847 (1982).
[202]V. E. Zakharov and E. A. Kuznetsov, Sov. Phys. JETP **39**, 285–286 (1974).
[203]I. Kourakis and P. K. Shukla, Phys. Rev. E **69**, 036411 (2004).
[204]T. S. Gill, C. Bedi, and A. S. Bains, Phys. Plasmas **16**, 032111 (2009).
[205]S. Sultana and I. Kourakis, Plasma Phys. Controlled Fusion **53**, 045003 (2011).
[206]E. A. Kuznetsov, A. M. Rubenchik, and V. E. Zakharov, Phys. Rep. **142**, 103–165 (1986).
[207]A. A. Mamun, S. M. Russell, C. A. Mendoza-Briceño, M. N. Alam, T. K. Datta, and A. K. Das, Planet. Space Sci. **48**, 163–173 (2000).
[208]A. R. Seadawy, Comput. Math. Appl. **67**, 172–180 (2014).
[209]A. R. Seadawy and D. Lu, Res. Phys. **6**, 590–593 (2016).
[210]C. S. Jao and L. N. Hau, New J. Phys. **17**, 053047 (2015).
[211]D. Mihalache and D. Mazilu, Rom. Rep. Phys. **60**, 957–975 (2008), see http://www.rrp.infim.ro/2008_60_4/04-957-975.pdf.
[212]G. Gottwald, R. Grimshaw, and B. A. Malomed, Phys. Lett. A **248**, 208–218 (1998).
[213]S. R. Sharma and R. S. Tiwari, Phys. Lett. A **57**, 341–342 (1976).
[214]E. W. Laedke and K. H. Spatschek, Phys. Rev. Lett. **47**, 719–722 (1981).
[215]N. S. S. Shalini and A. P. Misra, Phys. Plasmas **22**, 092124 (2015).
[216]A. B. Mikhalovskii, V. P. Lakhin, G. Onishchenko, and A. I. Smolyakov, Sov. Phys. JETP **61**, 469–475 (1985).
[217]V. I. Karpman, Phys. Scr. **20**, 462 (1979).
[218]V. I. Karpman, Phys. Lett. A **284**, 238–246 (2001).

[219]A. Mälkki, H. Koskinen, R. Boström, and B. Holback, Phys. Scr. **39**, 787–793 (1989).
[220]W. Lotko and C. F. Kennel, J. Geophys. Res. **88**, 381–394, https://doi.org/10.1029/JA088iA01p00381 (1983).
[221]W. Lotko, J. Geophys. Res. **91**, 191–203, https://doi.org/10.1029/JA091iA01p00191 (1986).
[222]C. Barnes, M. K. Hudson, and W. Lotko, Phys. Fluids **28**, 1055–1062 (1985).
[223]S. Qian, W. Lotko, and M. K. Hudson, J. Geophys. Res. **94**, 1339–1346, https://doi.org/10.1029/JA094iA02p01339 (1989).
[224]J. P. Crumley, C. A. Cattell, R. L. Lysak, and J. P. Dombeck, J. Geophys. Res. **106**, 6007–6015, https://doi.org/10.1029/2000JA003038 (2001).
[225]J. Dombeck, C. Cattell, J. Crumley, W. K. Peterson, H. L. Collin, and C. Kletzing, J. Geophys. Res. **106**, 19013–19021, https://doi.org/10.1029/2000JA000355 (2001).
[226]R. J. Strangeway, L. Kepko, R. C. Elphic, C. W. Carlson, R. E. Ergun, J. P. McFadden, W. J. Peria, G. T. Delory, C. C. Chaston, M. Temerin, C. A. Cattell, E. Möbius, L. M. Kistler, D. M. Klumpar, W. K. Peterson, E. G. Shelley, and R. F. Pfaff, Geophys. Res. Lett. **25**, 2065–2068, https://doi.org/10.1029/98GL00664 (1998).
[227]J. P. McFadden, C. W. Carlson, R. E. Ergun, D. M. Klumpar, and E. Moebius, J. Geophys. Res. **104**, 14671–14682, https://doi.org/10.1029/1999JA900035 (1999).
[228]Q. M. Lu, D. Y. Wang, and S. Wang, J. Geophys. Res. **110**, A03223, https://doi.org/10.1029/2004JA010739 (2005).
[229]P. K. Shukla, A. A. Mamun, and B. Eliasson, Geophys. Res. Lett. **31**, L07803, https://doi.org/10.1029/2004GL019533 (2004).
[230]C. S. Dillard, I. Y. Vasko, F. S. Mozer, O. V. Agapitov, and J. W. Bonnell, Phys. Plasmas **25**, 022905 (2018).